University of Zurich[UZH]

Department of Geography

Master's Thesis GEO 511

A Geochronological Reconstruction of Tsunami-Events Triggered by the Eqip Sermia in West Greenland

Author

Sutter Larissa Lucille

12-713-178

Supervised by:

Prof. Dr. Egli Markus, Geochronology UZH

Prof. Dr. Vieli Andreas, Glaciology UZH

Dr. Gärtner Holger, Dendrochronology WSL Institution,

Zürcherstrasse 111, 8903 Birmensdorf; holger.gaertner@wsl.ch

Faculty representative:

Prof. Dr. Egli Markus

September 2017

Department of Geography, University of Zurich

Abstract

Arctic regions are very sensitive to climate warming. Atmospheric and oceanic rising temperatures lead to dramatic changes in the dynamics of tidewater glaciers in Greenland. The Eqip Sermia in West Greenland is investigated since 1912. Due to the calving of the glacier terminus, tsunamis up to 20 m a.s.l. have been triggered. These tsunami-events can be detected with geochemical and dendrochronological analysis by investigating the mire-like and sandy soils and dwarf shrubs like Betula Nana and Salix Arctica. With LOI, XRF, C/N ratios, pH values and radiocarbon-data, information about the soils were gained. Annual ring widths of the dwarf shrubs were measured and cross-dated. The results only show relative and qualitative data, because correlations with the geochemical analysis and ^{14}C results could not be determined and the dwarf shrubs could not be cross-dated with a representative reference. Nevertheless, the radiocarbon-dating dated the beginning of the soil formation back to 9550 – 9494 cal. BP. This result suits to the global deglaciation history. Furthermore, recent ages were measured with ^{14}C that indicates disturbances during soil formation, presumably by cryoturbation rather than tsunamis.

Table of contents

I List of figures

II List of tables

III List of abbreviations

Units		Elements		Other	
Gt	Gigatons	**Na**	Sodium	**LOI**	Loss on Ignition
d	days	**Mg**	Magnesium	**AAA**	acid-alkali-acid treatment
a	years	**Al**	Aluminium	**AMS**	Accelerator Mass Spectrometry
ka	thousand years	**Si**	Silicon	**BN**	Betula Nana
cal.	calibrated age	**P**	Phosphorus	**SA**	Salix Arctica
BP	before present (1950)	**K**	Potassium	**H2O2**	Hydrogen peroxide
AD	after Christ	**Ca**	Calcium	**CO2**	Carbon dioxide
		Ti	Titanium	**H2O**	Water
		Mn	Manganese	**SO2**	Sulfur dioxide
		Fe	Iron	**CaCl2**	Calcium chloride
		U	Uranium	**CuO**	Cupric oxide
		C	Carbon	**a.s.l.**	above sea level
		H	Hydrogen	**ETHZ**	Swiss Federal Institute of Technology Zurich
		N	Nitrogen		
		Zr	Zirconium		
		Rb	Rubidium		

1. Introduction

While climatic warming can be observed globally, the Arctic environment reacts extremely sensitive to the changing climate (IPCC, 2014). In the past few years, accelerated glacier melting was observed in Greenland due to climatic warming. Tidewater glaciers respond with thinning at their terminus, retreat and higher iceberg calving rates (Rignot et al., 2010; Amundson et al., 2008). The higher air temperature leads to a greater production of melt water at the glacier surface, which runs into crevasses and favours instability of the glacier terminus (Scambos et al., 2000). In addition, higher ocean temperatures enhance the instability due to submarine melting (Rignot et al., 2010). Outlet glaciers start to collapse at their front, which is known as the process of iceberg calving (Warren, 1993). Calving events can cause large and hazardous tsunami waves, which erode the soil and destroy the vegetation and infrastructure on the shore (Lüthi & Vieli, 2016).

The Eqip Sermia in West Greenland is a very well investigated tidewater glacier. Measurements of flow-speed and the geometry of its terminus reach back to 1912 (Lüthi et al., 2016). Tsunamis, caused by calving, were documented since 1912 as well (Lüthi et al., 2016). Thus, these tsunami-events are not newly discovered phenomena. Since 2012, the calving front has shown a special geometry that causes large tsunami waves with heights up to 20 m a.s.l. in a single calving-event. These destructive tsunamis have not been observed before, making it to a recent unprecedented phenomenon in the history of this glacier (Lüthi & Vieli, 2016).

Since bogs and peaty soils may persist up to thousands of years, they act as reliable archives for environmental changes (Kylander et al., 2013). The soils at the Eqip Sermia are either eroded or conserve footprints of tsunami-events. These soils can be analyzed using geochronological methods. Another possible archive for recent environmental changes are dwarf shrubs. They form annual rings, whose variability in width is influenced by environmental conditions (Schweingruber, 1996). Therefore, it can be assumed, that tsunami-events can be tracked using geochemistry, radiocarbon-dating and dendrochronology.

This Master's Thesis uses soil parameters, radiocarbon-dating and dendrochronology to investigate, if these destructive tsunamis; caused by calving from the Eqip Sermia, can be measured in the soil formation and in the dwarf shrubs.

This experimental Master's Thesis focusses on the following research questions:

- *"How suitable is the geochemical analysis of mire-like and sandy soils, radiocarbon-dating and the dendrochronological analysis of the dwarf shrubs Betula Nana (BN) and Salix Arctica (SA) to deduce tsunami-events?"*
    - *H_0 = Mire-like and sandy soils and the dwarf shrubs BN and SA are suitable to trace tsunami-events.*

According to the staff working at the Eqip Sermia, big tsunamis occur since 2012. It is assumed, that the special geometry of the calving front is responsible for big tsunamis since 2012. If the geochronological methods are useful for detecting tsunami-events, a further research question calls of an answer:

- *"Have other large tsunami-events, caused by calving of the Eqip Sermia, occurred before 2012?"*
    - *H_0 = Large tsunami-events have not occurred before 2012.*

If big tsunamis manifested themselves only after 2012, it would verify the hypothesis of Lüthi et al. (2016), that this special geometry of the calving front (see chapter 3.1.2.) formed in 2012 (Lüthi & Vieli, 2016), is the main reason for this phenomenon.

Another research question in this Master's Thesis is:

- *"Is it possible to measure the quantity of tsunami-events?"*
    - *H_0 = The quantity of tsunami-events is measurable.*

2. Basics

2.1. Climatic warming and tidewater glaciers

The Arctic region can either be defined by the air temperature, the tree line or the latitude. Whereby the average air temperature in July stays below the 10°C mark and at the same time the tree line follows more or less this air temperature line (Kappas, 2009). The latitude of 66,5°N defines geographically the Arctic circle (Kniveton, 2007). The global climate is strongly influenced by the Arctic. It regulates the global water cycle and especially oceanic currents (IPCC, 2014). The Arctic environment reacts extremely sensitive to the changing climate and is the most vulnerable region regarding global warming (IPCC, 2014). Due to interactions between ice, snow, atmosphere, ocean and land in the Arctic and various feedback processes linked to these interactions, the Arctic is a highly complex and sensitive region (Hansen et al., 2006).

The average air temperature in the Arctic has increased more than twice as fast as the global mean during the past century and is estimated to continue with this rate (Weijers et al., 2013; IPCC, 2014). During the last 30 years, the air temperature in the Arctic has risen 2°C on average (Jia et al., 2009). The strongest climatic warming for the next decades will occur at high latitudes (Blok et al., 2011). Climate predictions suggest a continuous increase in air temperature, which has the strongest effects in winter due to changes in snow budget (Hollesen et al., 2015).

This climatic warming is a clear sign of an anthropogenic greenhouse effect (Serreze et al., 2006). As a result, permafrost is thawing, the sea ice is melting and glaciers are retreating (IPCC, 2014). Due to the increased emission of greenhouse gases, a positive feedback mechanism is generated. The air temperature is rising, consequently snow and ice is melting and hence, results in a reduced albedo. Thus, more short wave radiation from the sun can be absorbed, which leads to a further warming of the global air temperature and therefore, causes increasing glacier retreat and snow melting (Bradley et al., 2006).

Most terrestrial glaciers can be used as an indicator for climate changes in the past and present. For climatic interpretations, based on the behavior of glaciers, representative glaciers are necessary (Post et al., 2011). But debris-covered or tidewater glaciers react differently to the changing climate. Tidewater glaciers originate in the mountains, terminate in the sea and are grounded on the seafloor. Theses glaciers do not belong to the representative glaciers, because of their asynchronous behavior in climatic context (Post et al., 2011). Nevertheless, the rapid retreat of

tidewater glaciers in Greenland seem responsive to climate change, due to the correlation between the rise of air temperature and retreat of these glaciers (Moon & Joughin, 2008; Nick et al., 2013). One of the most dominant reactions of the outlet glaciers is their acceleration of glacier movements, due to an increase in surface melt around Greenland (Moon & Joughin, 2008; Rignot et al., 2010). The acceleration of these glaciers are strongly connected with the calving terminus and the thinning mechanism (Juan et al., 2010; Howat et al., 2008). Through the process of iceberg calving, a reduction of resistive stresses at the terminus occurs and results in acceleration of the glacier (Juan et al., 2010). The calving induced velocity increases near the glacier terminus is ~ 3% (Amundson et al., 2008). This calving mechanism is an important factor in mass loss on the Greenland ice sheet (Amundson & Truffer, 2010).

Approximately 84% of the area of Greenland (2,2 million km^2) is covered with ice (Walker et al., 2005). In Greenland, 90% of the ice discharge into the ocean is controlled by the outlet glaciers. The entire mass balance of the ice sheet is therefore largely affected by submarine melting (Rignot et al., 2010). Between 1992-2001 and 2002-2011 the mass loss of the Greenland ice sheet has quadrupled from 51 ± 65 Gt a^{-1} to 211 ± 37 Gt a^{-1} with increasing tendency (Straneo & Heimbach, 2013; Lüthi et al., 2016). 50-60% of increasing mass reduction around Greenland, in the past decades, is caused by an acceleration of the tidewater glaciers (Rignot et al., 2010). Whereas the warmer air temperature thins the glacier from the surface, warmer ocean temperature leads to a retreat of the grounding line, due to eroding of the submerged grounded ice (Rignot et al., 2010; Lüthi et al., 2016; Amundson et al., 2008).

2.2. Geochronology

2.2.1. Geochemistry and age determination

The ice sheet of Greenland started to grow with the cooling during Cenozoic. Until the start of the deglaciation in the early Holocene, 10'500–10'000 years before present (= 10.5 ka–10 ka BP), a number of interglacial periods have been documented (Weidick et al., 2007). During the Little Ice Age, the ice sheet started to advance again and reached its neoglacial maximum around 1850 AD. Since then the re-advance was interrupted by a recession in the ice sheet that continues to the present and future. As a consequence of the rapid deglaciation during early Holocene, lakes were formed. With an advanced vegetation and soil formation, these lakes disappeared (Veit, 2002). During the sedimentation of these lakes, signals of the surrounding environment were conserved (Gierlowski-Kordesch, 2004). Due to of the stratigraphy caused by sedimentation that leads to a rising surface with every life sequence of plants and because of

water, that shows neither horizontal nor vertical movements, the oldest matter lies at the bottom; while the newest is at the surface. Hence, these soils act very well as archives for environmental changes over a long time period (Musso, 2016; Logsdon, 2008).

With techniques from the geochronology soils can be investigated. Biological, physical, and chemical dating methods are used. A very common method that gained a lot of attention in the past is palynology for investigation of mires. It is used to reconstruct the vegetation cover by analyzing pollen (Jäger, 2013). Further methods for relative and absolute dating are dendroecology and dendroclimatology, Loss-on-ignition (LOI), ratios of carbon and nitrogen (C/N), pH, bulk density for the accumulation rate, stable isotope analysis, dendrochronology, radiocarbon-dating, x-ray fluorescence (XRF) and more (Chambers & Charman, 2004).

With the chemical analyzer (XRF) several investigations can be conducted. For investigations of weathering processes the elements Na, Al, Si, K and Fe are the most important (Jäger, 2013). But even more common for weathering indices are ratios between easily leachable (Ca, Mg, K, Na) elements to less mobile elements (Al, Fe, Si, Ti etc.) (Boxleitner et al., 2017). Water is an important medium for chemical weathering. Over a long time, water continuously dissolved salts and minerals from the parent rock. This leads either to a leaching or a fixing of elements by forming secondary minerals (Musso, 2016). For this Master's Thesis Na, Si and the molar ratio of (Ca+K)/Ti are used for analyzing weathering processes and K/Rb for the aeolian flux and lithogenic sources. The more the ratio varies within a soil profile the more different lithogenic sources exist. The lower the molar ratio of (Ca+K)/Ti the higher the weathering and therefore the older the sample (Boxleitner et al., 2017; Egli et al., 2008). On stable soil surfaces the most weathered material should be measured there, due to the weathering process from the surface to the bottom. Thus a low molar ratio of (Ca+K)/Ti is found in these materials (Boxleitner et al., 2017).

Since the soils at the Eqip Sermia are not mires itself, but mire-like and sandy soils, techniques from geochronology should be adaptable. The methods used for this Thesis are limited on LOI, pH, C/N ratio and XRF, that depend on chemical features or changes in their amount over time and depth (chapter 4.2.1.), dendrochronology that focuses on growth layers of a plant (chapter 2.2.2.) and radiocarbon-dating for age control of the chemical analysis (Chambers & Charman, 2004).

The chemical and biological methods are used for the determination of rather recent ages compared to the radio isotopic method. Ages back to 50 ka can be determined with this method and is based on the half-life period of the radioactive isotope radiocarbon (^{14}C). The ^{14}C β decay half-life (= $T_{1/2}$) is 5720 ± 30 a (Fig. 1) (Piotrowska et al., 2011; Reimer et al., 2013). Radiocarbon-dating is the most common dating technique for age reconstructions at the Late Pleistocene and Holocene (Piotrowska et al., 2011).

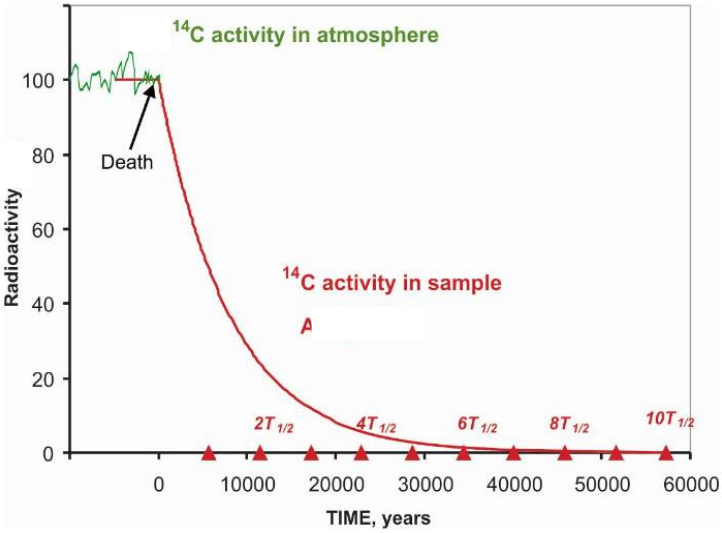

Figure 1: *Radiocarbon activity changes in organisms initially absorbing carbon from the atmosphere, dying at TIME = 0 and being incorporated into a mire or soil sample (Piotrowska et al.,2011).*

^{14}C has its origin in the upper atmosphere and is produced by cosmic radiation (Musso, 2016). The atmospheric carbon dioxide (CO_2) contains only a small amount of ^{14}C, whereby stable isotopes ^{12}C and ^{13}C appear in higher concentrations. CO_2 gets absorbed by organisms with a $^{14}C/C$ ratio, that is in equilibrium with the atmospheric ratio (Blaauw & Christen, 2005). Due to the radioactive decay, the $^{14}C/C$ ratio starts to decrease when the organism dies, as the carbon exchange ceases. Hence, the $^{14}C/C$ ratio can be measured in fossil organisms which allows determining its radiocarbon age (Fig. 1a). However, this age is not absolute, due to errors while measuring ^{14}C and due to an inconstant radiocarbon production over time. Calibrations to calendar ages are necessary for corrections of the radiocarbon age (Blaauw & Christen, 2005; Musso, 2016). The calibrated age is given in ranges with probabilities (1σ = 68,2%, 2σ = 95.4%), due to uncertainties while measuring and calibration.

2.2.2. Dendrochronology

2.2.2.1. Wood anatomy

Dendrochronology is very interdisciplinary and is used in various research fields like archeology, climatology, geomorphology, tectonics, ecology, glaciology, snow research and more (Schweingruber, 1988; Schweingruber, 1996; Young et al., 2016). All parts of a tree (roots, stem, branches) react to the surrounding environment. When the environmental conditions are changing, the trees adapt immediately. These responses can be observed in their annual rings,

which will be explained in more detail later. Due to their lifespan, varying from a few decades up to a few thousands of years, trees can be used as archives for environmental changes (Schweingruber, 1988). A pioneer in dendrochronology is A. E. Doulgass (1867–1962), who recognized that the structure of tree-rings can be used for dating determinations (Becker, 1992). Therefore, he developed the cross-dating method and laid the basis for dendrochronology. The cross-dating method compares characteristics of annual rings of minimum two plants with the aim to assign years to specific rings (Wimmer, 2002). Further he evolved methods for reconstructing the past climate by observing variations of tree-rings (Becker, 1992).

The development of wood is influenced by climatic conditions. With the beginning of the vegetation period the cell division starts in the cambium. The xylem is build inwards, whereas the phloem is build outwards. The primary cell wall synthesis indicates the start of the cell development, followed by the secondary wall synthesis, a thickening and lignification of it (Li et al., 2010). The growth interruption caused by climatic conditions is decisive for the characteristics of the annual rings. This seasonal activity of the cambium leads to annual rings which can be distinguished in earlywood and latewood (Li et al., 2010). Depending on the latitude and altitude, earlywood is produced in spring and early summer. On the contrary, latewood is formed between late summer and autumn (Paiva et al., 2008; Shroder, 1980). The tracheids of earlywood are lager in its lumen dimension compared to latewood and they are formed with thinner walls. This is due to the transport of water, which is important during spring and early summer. The walls of the cell get thicker in latewood and is responsible for the stability of the plant and mechanical strength (Fig. 2).

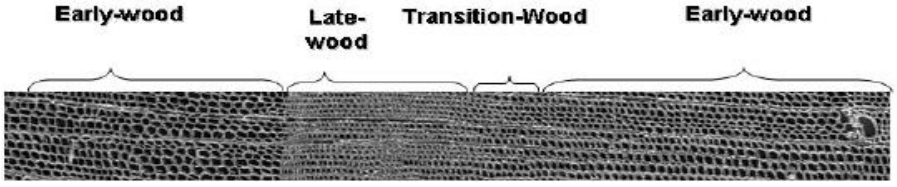

Figure 2: *Cellular structure of earlywood and latewood of a conifer (Kretschmann & Cramer, 2007).*

Hence, the largest difference of wood properties can be seen at the transition from earlywood to latewood (Camarero et al., 1998; Li et al., 2010). This anatomical difference makes it possible to distinguish the single vegetation periods of trees, shrubs and dwarf shrubs (Schweingruber & Poschlod, 2005). Not only the age can be determined, also climatic and other environmental influences and changes of internal factors, like soil condition or pollution and more are reflected in annual rings (Camarero et al., 1998).

3. Investigation area

3.1. History of Eqip Sermia

3.1.1. Isostatic response

During the Wisconsian Ice Age (25 ka–21 ka) the last glacial maximum was reached. At this time, the global sea level was 130 m below present. As mentioned in chapter 2.2.1. the deglaciation in Disko Bugt started around 10.5 ka BP. During early Holocene, a rapid relative sea-level fall was reported, followed by a slow rise in late Holocene. This phenomenon is the direct isostatic response to the development of the ice sheet (Weidick et al., 2007). The relative sea-level has also been dated. Marine terraces were found at an elevation between 70–80 m a.s.l. with an age of about 10–9 ka BP. This age correlates with the minimum age within the last deglaciation. At a height of 30 m a.s.l. a shell was dated back to 7.7 ka BP. It is assumed, that this shell sample is related to the marine sea level around this elevation (Weidick et al., 2007). Figure 3 shows an example of two relative sea-level curves from Disko Bugt, whereas the Eqip Sermia is located in the north-eastern part of Disko Bugt (see also Fig. 5). Due to the thinning of the Inland Ice in this area, the present vertical crust movements vary between +1.6 mm a^{-1} and +4 mm a^{-1} (Weidick et al., 2007).

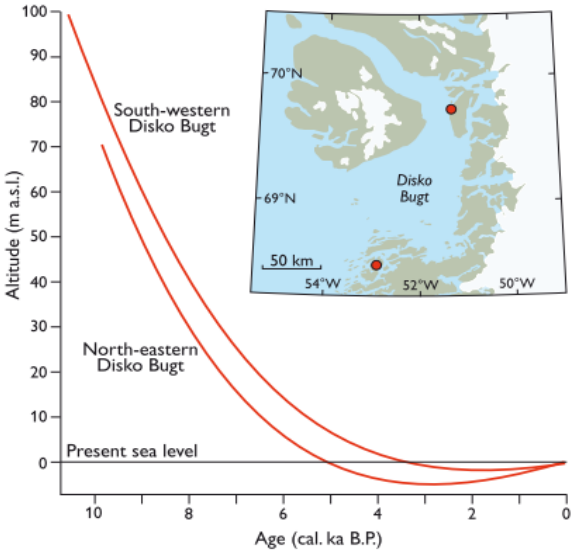

***Figure 3**: Two curves of the relative sea-level at Disko Bugt (Weidick et al., 2007).*

3.1.2. Development of the Eqip Sermia

The Eqip Sermia is well accessible and located on a main route for scientific expeditions to the ice sheet. Therefore, documentations of ice velocity, terminus position (Fig. 4) and surface topography of the Eqip Sermia were made during the whole 20th century (Lüthi et al., 2016). First investigations started with Alfred de Quervain and Paul-Louis Mercanton in 1912, followed by scientific expeditions with the German *Alfred Wegner Expedition* between 1929 and 1931. This work was continued by the *Expéditions Polaires Françaises* (EPF 1948–1953). They conducted mass-balance measurements along an east-west profiles from coast to coast over the central part of Greenland, described the area at the Eqip Sermia and mapped of the ice sheet margin nearby

(Weidick et al., 2007; Lüthi et al., 2016). A further expedition was the *Expéditions Glaciologiques Internationales au Groenland* between 1957 and 1960, followed by smaller expeditions in 1971, 2005, 2007, 2008, 2011 and 2013 (Lüthi et al., 2016).

Between 1912 and 1929 the glacier reached its recent maximal extent, whereas the glacier advanced by ~ 400 m. It is estimated that the advance of the glacier stopped at 1920 (Nielsen, 1992; Lüthi et al., 2016). Until the 1960s the terminus retreated 1.3 km, followed by a slow and continuous advance until 1990 (Lüthi et al., 2016). The terminus retreated another 0.5–1 km until 2004. The minimum position between 1950 and 1975 was reached again in 2010 and additionally a rapid retread of 1–2 km occurred until 2015. The velocity close to the terminus in the late 1950s was 3.6 m d^{-1}. An increase in velocity of 30% was determined between 2000 and 2005 (Maas et al., 2007). The terminus flow velocity reached its maximum in 2014 with 15 m d^{-1} (Lüthi et al., 2016).

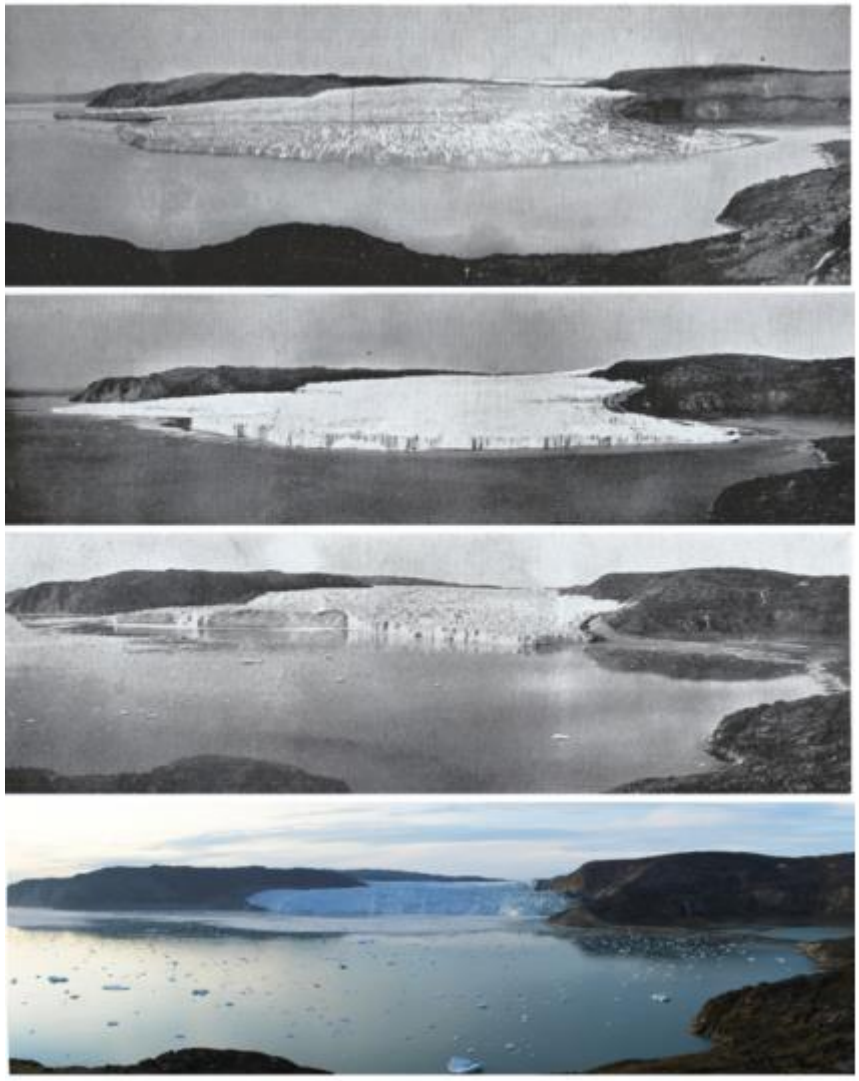

***Figure 4**: Photographs of the terminus position of the Eqip Sermia in 1912, 1929, 1953 and 2015 (Lüthi et al., 2016).*

While the glacier front of tidewater glaciers usually reaches heights of < 100 m and have a relatively vertical and floating position, the geometry situation of the Eqip Sermias central front is exceptional, because of its height of ~ 200 m and an inclination of the front of 45° resting on the glacier bed. This special geometry might be responsible for the recent phenomenon of large tsunami-events caused by a collapsing glacier front with volumes up to 10^5 m^3. (Lüthi et al., 2016)

The oceanic influence on the future evolution of the Eqip Sermia is still uncertain. But it is certain, that future development is determined by the calving dynamics and topography of the glacier bed. The bedrock on which the glacier front is currently resting, turns into a 200–400 m below sea level deep sink with a length of 10 km, where it reaches an up-sloping bed. Future retreat rates of the Eqip Sermia are assumed to be extreme in the next decade. (Lüthi et al., 2016)

3.2. Climate and geology

As shown in Figure 5, the glacier Eqip Sermia is located in central West Greenland (69°47'N, 50°15'W) (Maas et al., 2007). The climate is characterized by an arctic maritime climate with an average air temperature of 7.1°C in July and an average precipitation of 436 mm per year (Hansen et al., 2006). The geology of West Greenland of the investigated area is characterized by the Precambrian. The most common crystalline rocks in this area are granites, orthogenesis but also sedimentary and volcanic rocks with signs of metamorphosis (Weidick et al., 2007). A sedimentary basin was formed because of a down-faulting and a parallel rifting to today's coastline in West Greenland during the Mesozoic. This was caused by the fragmentation of the Precambrian shield due to the movements of the plate tectonic (Weidick et al., 2007). During the Cenozoic, West Greenland was uplifted by epeirogenesis. Cycles of this genesis and erosion are responsible for the present morphology of West-Greenland and therefore also for study site (Weidick et al., 2007). The soil characteristics vary from dry and sandy soils to mire-like soils. Further description about the soil and the different profiles can be looked up in chapter 5.1.1.

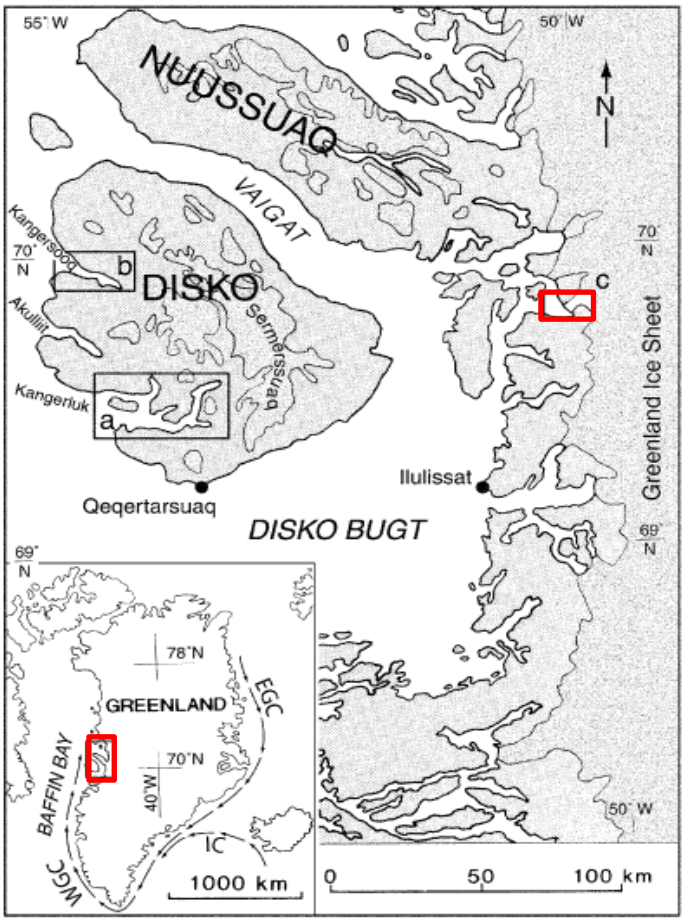

Figure 5*: Location of the Eqip Sermia glacier (Desloges et al., 2002).*

3.3. Dwarf shrubs

Dwarf shrubs are perennial and woody plants, which can be very persistent up to centuries. Due to the seasonal climate, distinguishable annual growth rings are formed. These rings are used for different analysis methods (see chapter 2.2.2.) (Myers-Smith et al., 2015a). The radial growth is mainly driven by the warmth in summer. In West Greenland, the vegetation period is between June and July, when temperature is ≥ 5°C, which is the minimum temperature for plant growth (Hollesen et al., 2015; Weijers et al., 2013). This short vegetation period and the low arctic temperatures lead to a small radial growth of dwarf shrubs. But these conditions additionally increase the lifetime of plants (Schweingruber et al., 2013).

BN and SA are both circumpolar species and can be found on coastal regions in West Greenland (Groot et al., 1997; Schmidt et al., 2006). They are dwarf shrubs and reach up to 30 cm height. BN belongs to the birch species and prefers moist and elevated soils (Blok et al., 2011; Groot et al., 1997). The willow species SA prefers drier soil and has well-defined annual rings similar to BN. Nevertheless, both species cause issues for cross-dating due to discontinuous or even missing rings (Groot et al., 1997; Schmidt et al., 2006). Figure 6 shows a portrait of a) BN and b) SA.

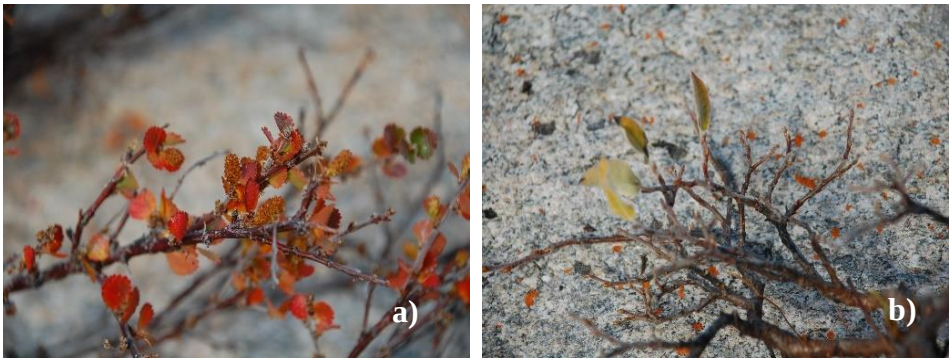

***Figure 6**: a) shows the BN species and b) is the SA.*

4. Material and Methods

4.1 Field work

The field work took place between the middle and the end of August 2016. Dr. Martin Lüthi and Prof. Dr. Andreas Vieli from the University of Zurich are leading research projects at the Eqip Sermia. Their knowledge has been helpful at choosing a suitable investigation area.

4.1.1 Selection of the investigation area

It was of utter importance, that the area is affected by tsunamis, that are triggered by the Eqip Sermia. Therefore, the coast on the left side of the tidewater glacier became the investigation area as shown in Figure 7.

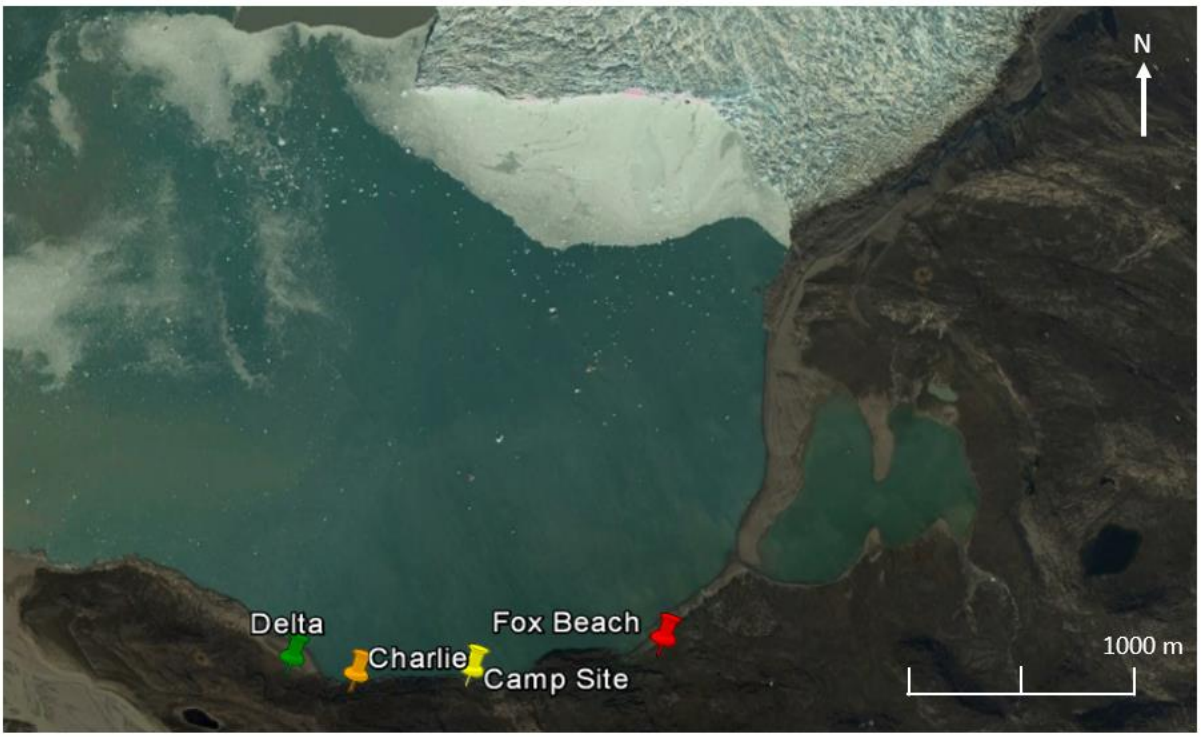

Figure 7: *Site distribution. Eqip Sermia glacier with the sites Fox Beach, Camp Site, Charlie and Delta using Google Earth.*

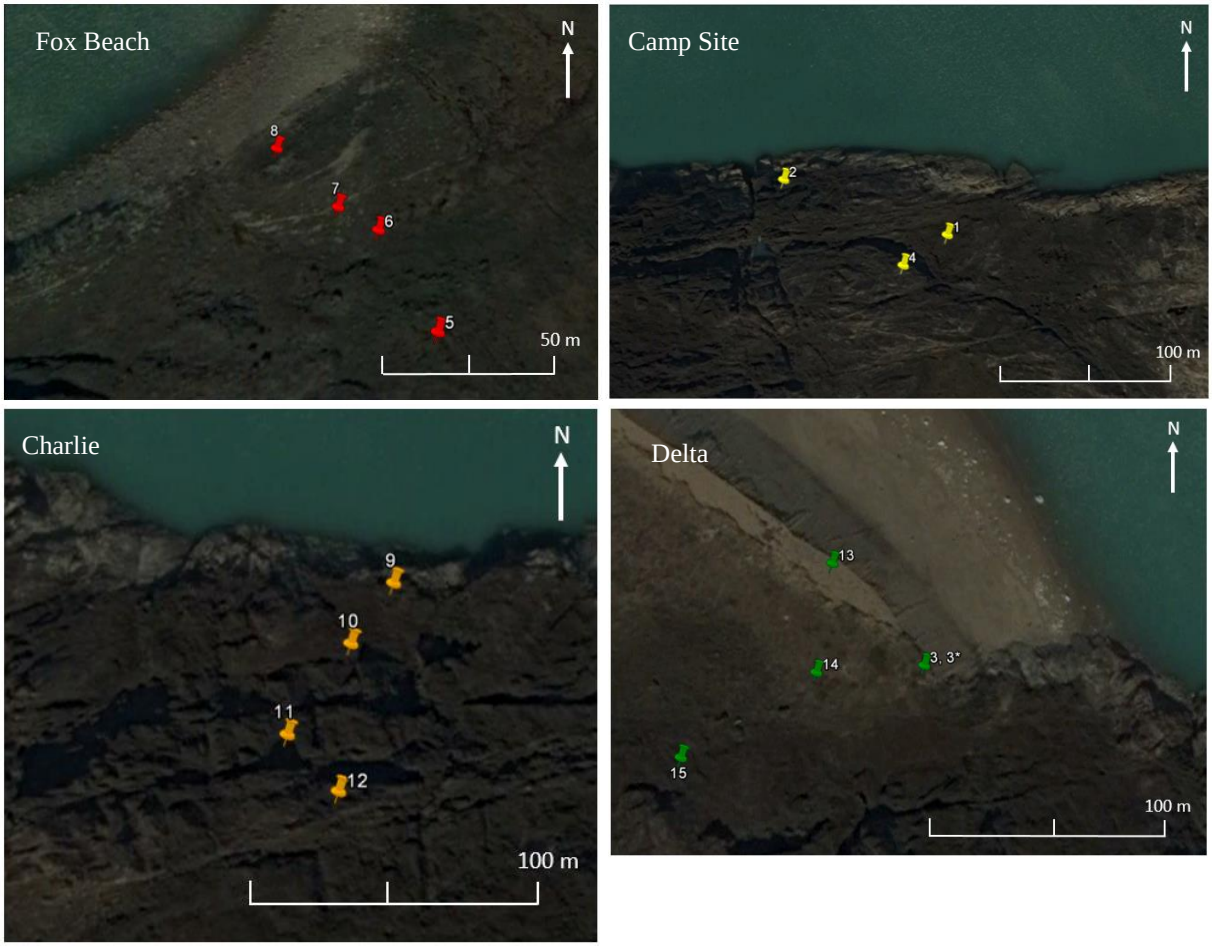

Figure 8: *Sample distribution. Fox Beach with the four sampled profiles 5, 6, 7, 8 (red). Camp site with the three sampled profiles 1, 2, 4 (yellow). Charlie with the four sampled profiles 9, 10, 11, 12 (orange). Delta with the five sampled profiles 3, 3* 13, 14, 15 (green) using Google Earth.*

The investigation area was distinguished in four main sites. First, Fox Beach (red) (Fig. 7 and 8) which was chosen due to the gradual slope, the continuity of topography, the large area and the visual differences of the vegetation. Additionally, this site starts at sea level, which makes it to an interesting site.

Another site is Camp Site (yellow) (Fig. 7 and 8). This site is attractive to sample because of the presence of a terrace. At the same time, human activity is the highest at this place, because boats are docking here, which can be hit by tsunamis.

The third main site is Charlie (orange) (Fig. 7 and 8). Due to an interesting formation in the soil, Charlie was sampled. This site starts at a higher elevation. The slope at this site is very steep compared to the other sites. Therefore, the samples were taken very close to each other. But there were still observable differences in the vegetation.

The last one is Delta (green) (Fig. 7 and 8). With 22 m a.s.l., Delta is placed the highest, which makes it to another interesting spot for investigations. It is directly located above a sandy coast cliff.

Each of these main sites were divided into zones as shown in Figure 9 at Fox Beach:

Figure 9*: Zone definition at Fox Beach with the four zones: (5) is the reference, (6) the transition, (7) the affected and (8) the dead zone.*

A reference zone (5), which was not affected by tsunamis. This zone was either far away from the coast or at a higher elevation. The vegetation in this zone was fully intact. A transition zone (6) between the affected part and the part which was not affected by tsunamis. A probably affected zone (7), where the vegetation is still alive and a dead zone (8). This zone is obviously affected by tsunami-events because of dead vegetation and erosion of the soil. Furthermore, sediment and rock fragment deposits are accumulated.

4.1.2. Sample collection

Due to the high occurrence of BN and SA, it was decided to sample these species. At each site and zone, one to two species BN and SA have been carefully excavated. A total of 12 BN and 10 SA samples have been collected. Plant and soil formation are strongly connected to each other. Therefore, soil and plant samples should be together as close as possible. Further it can be assumed that the same environmental conditions are dominant. For the soil samples, a profile down to the bedrock was dug. The profiles were sampled every 2,5–5 cm, depending on the depth of the soil.

4.2. Laboratory work

4.2.1 Geochemistry and radiocarbon-dating

4.2.1.1. Soil preparation

First, the weight of all samples was determined before they were dried in an oven for 24 h at 70°C. After the drying process, the soil weight was measured again to calculate the moisture in the soils and to attain the dry weight of the soils. As for the geochemistry, only fine earth material < 2 mm is needed. However, a sieving of the samples was not necessary, because the soil did not contain any bigger material than 2 mm. An amount of this material was milled with a horizontal machine using two tungsten balls (Egli et al.,2016).

4.2.1.2. Loss on Ignition

For the analysis of the organic part in the samples, 2 g of the non-milled, oven-dried soil sample was weighted out into porcelain crucible and then burnt at 550 °C for six hours in an oven. Then the weight difference has been recorded, to obtain the quantity of organic material (Egli et al., 2016).

4.2.1.3. X-ray fluorescence spectroscopy

The x-ray fluorescence (XRF) spectroscopy is a chemical analyzing method that does not destruct the sampled material. It is capable to measure the concentration of most elements from Na and to U on the periodic table. It is used to analyze the chemical structure and therefore, gain information about trace elements (Na, Mg, Al, Si, P, K, Ca, Ti, Mn, Fe) in the fine-grained soil samples. The sum of these trace elements represents the total content of inorganic matter. Other elements can be ignored, due to their small amount (Musso, 2016). 5 g of the milled soil of each sampled horizon was added in small plastic containers and irradiated with x-rays in the XRF spectrometer. As result, the quantity of each trace element and further elements of every sample could be determined (Egli et al., 2016).

4.2.1.4. Hydrogen ion concentration measurements

Figure 10: *Samples prepared for pH-measurements with a magnet stirrer.*

To measure the hydrogen ion concentration (pH-value), a pH-meter and unmilled (< 2 mm) soil samples were used. Each sample was mixed with a solution of 0.01 mol g^{-1} $CaCl_2$ with a sample-solution ratio of (1:2.5). 2 to 5 g material was added in a breaker glass, depending on the suction of the material. Therefore, 5 to 12,5 ml of the solution was necessary for measuring the pH. This suspension was mixed with a magnet stirrer, which turned 250 times per min (Fig. 10). The mixing took 15 min and afterwards the samples rested for another 15 min. The pH-value was finally measured with a pH-meter (Egli et al., 2016).

4.2.1.5. CHN

2 mg of the fine milled soil, which was filled into tin-capsules, was needed to determine the organic C and N values from homogenous organic materials. For this a CHN-elemental analyzer from Leco (CHNS-932) was used. A heated oxygen-rich environment combusted the soil samples. CO_2, H_2O, N_2 and SO_2 resulted from this process. Whereas N_2 was measured by thermal conductivity, CO_2 and H_2O were removed by Lecosorb and Anhydrone. As a final result the weight percent of C, H and N was obtained (Egli et al., 2016).

4.2.1.6. Radiocarbon-dating

A selection of samples was dated with the ^{14}C method. The uppermost and the lowest horizons of four soil profiles and the lowest horizon of three soil profiles were dated. Depending on the

material, the sample was pretreated with 10% hydrogen peroxide (H_2O_2) for soil samples (< 2 mm) or using acid-alkali-acid treatment (AAA) for organic matter (Egli et al., 2016; Fumal et al., 1999).

To extract the oldest C fraction from the soil, H_2O_2 was used for the pretreatment. 2 g of the soil samples (< 2 mm) were soaked in distilled water for 10 min. Then 180 ml of 10% H_2O_2 was added. The duration of this treatment took 168 h (7 d) and ran at a temperature of 50°C. The last step of the treatment was washing the samples with 80 ml deionized water for three times. After that the samples were dried, weights recorded and the analysis for the total C and N content was determined before the samples were ^{14}C dated (Halpern, 2016). With this oldest C fraction, it is possible to estimate the approximate begin of the soil formation.

With the AAA, the CO_2 was absorbed in quartz tubes with CuO (oxygen source) and heated under vacuum. To separate the CO_2, a vacuum in the quartz tubes was created again, then sealed and heated in an oven at 900°C. The released CO_2 of the burnt sample was assorted with H_2 in a ratio of 1:2.5. After that mixing process, it was reduced to graphite at 535°C above iron powder. The Accelerator Mass Spectrometry (AMS) at the ETHZ measured the C ratios (Egli et al., 2015; Boxleitner et al., 2017).

The ^{14}C data were calibrated by using the OxCal 4.2. calibration program (Bronk Ramsey, 2001; 2009). It is based on the IntCal 13 calibration curve (Reimer et al., 2013) and for modern samples the Bomb 13NH1 curve was used (Hua et al., 2013). The calibrated ages are given in a rages of 68.2% (1σ) and 95.4% (2σ) probability, which are the minimum and maximum values (Piotrowska et al., 2011; Egli et al., 2015).

4.2.2. Dendrochronology

4.2.2.1. Sample preparation

Before the samples were taken to Switzerland, the dwarf shrubs were cut in to 2–4 cm big pieces in the field (Fig. 11). The stem was separated from the roots and branches. The roots and branches were sampled every 5 cm. All the samples were kept and transported in small paper bags. Due to the containing moisture in the plants, no plastic bags were used, as the samples could rot.

The most important piece, which was used for the dendrochronological analysis, was at the transition zone between root and shoot. This part of the plant was formed first and therefore, it potentially contains the oldest part of the plant and thus the most annual rings (Blok et al., 2011).

Figure 11: *BN species a) before and b) after cutting.*

The following steps were completed according to Schweingruber et al. (2013), Gärtner & Schweingruber (2013) and Myers-Smith et al. (2015b).

4.2.2.2. Cross-Sectioning

Before the cross-sections were made, the samples were cleaned with water and a brush to remove little stones and soil fragments. The samples were saturated in water to soften it and thus, making the sectioning easier. The blade was covered with water drops to ensure that the cross-sections would stick to the blade. With a wet brush, the cross-sections could be easily removed from the blade. They were then placed on a glass slide with glycerol. Glycerol prevents the sections from drying and preserves the samples until the dying process sets in. Several cross-sections of the stem, above and below ground have been made with a thickness between 8–30 µm using a sliding microtome (Fig. 12 a), b)). For the final analysis, the best cross-section was selected.

Figure 12: *a) Microtome with sample for cross-sectioning; b) cross-sections on glass slides.*

4.2.2.3. Dyeing and dehydration processes

Before dyeing (Fig. 14 a)), the samples were cleaned with water by a pipette. To enhance the contrast between the non-lignified and lignified cells, a staining solution of Astrablue and Safranin with a ratio of 1:1 was used. The Astrablue stain consists 2 ml acetic acid and 0.5 g Astrablue powder in 100 ml distilled water, whereas the Safranin stain consists 0.8 g Safranin powder in 100 ml distilled water. Astrablue stains the non-lignified cell walls blue and the Safranin the lignified cells red (Gärtner & Schweingruber, 2013). This double staining solution was dropped on the cross-sections and left for soaking at least 5 min before washing out.

After the dyeing process (Fig. 14 b)), the samples were dehydrated with ethanol, starting with 75% ethanol until the washed-out solution was colorless. The next step was to rinse the samples with 96% ethanol and at the end with 100% ethanol until the sections were uncolored. After dehydration Xylol was used to make sure, that the samples did not contain any water (Fig. 13). Additionally, Xylol dilutes the viscous Canada Balsam and was then able penetrate the cells of

the sample. If the sample still contained water, the Xylol changed its clearness to a milky solution. This process was repeated until the Xylol stayed clear. It is important, that no water was left in the cross-sections, because water has another light refraction index compared to glass and the Canada Balsam. Therefore, it would reduce the quality of the photographs. Before the samples were dried for 48 hours at a temperature of 60°C, the samples were embedded in Canada balsam and covered with a glass. While covering the samples with the glass, attention had to be paid on preventing the development of air pockets.

Figure 14: *All liquids needed for dyeing; water, double staining solution Safranin and Astrablue, ethanol 75%, 96% and 100% and Xylol.*

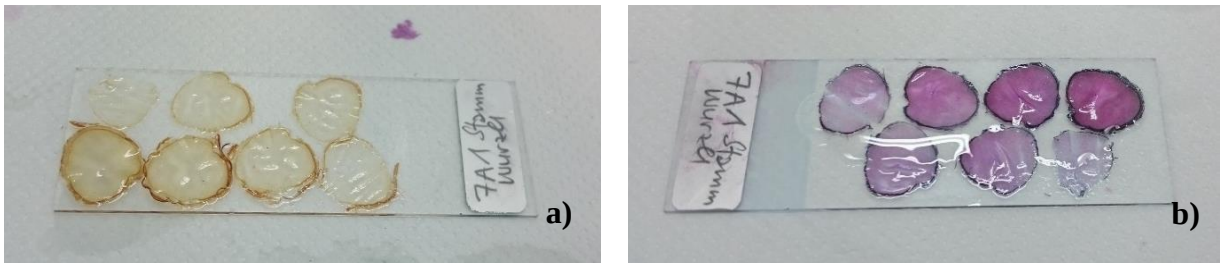

Figure 13: *Cross-sections a) before and b) after dyeing and dehydration process.*

4.2.2.4. Microscopic photographs

Since the dwarf shrubs contain microscopic narrow annual rings, a light microscope was used to take the photographs (Fig. 15). They were taken with a 40 times magnification. A higher magnification was not necessary, because the annual rings were clearly visible with the magnification of 40. The camera was connected with the computer, which eased the shooting. The cross-sections had to be photographed multiple times. All photos of a sample had to be stitched together to get a full image. At least the longest radius was photographed. Additionally, one to three more radii were shot.

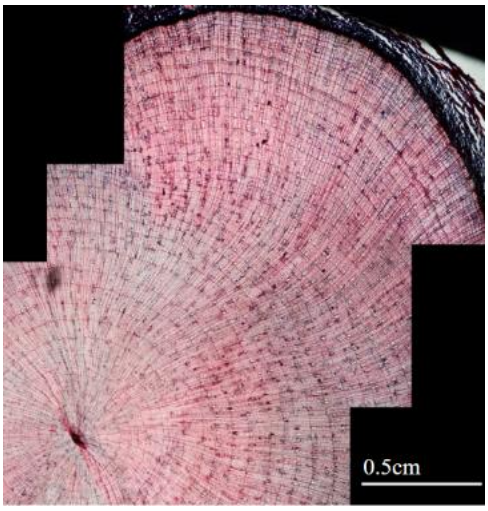

Figure 15: *Photographed cross-section with a microscope with a 40 times magnification.*

4.2.2.5. Ring width measurements with WinDENDRO

For the cross-dating and the detection of growth changes, the annual ring widths had to be measured. For these measurements, the software *WinDENDRO* was used (Fig. 16). Due to discontinuous or even missing annual rings it was important, that more than one radius was measured (Schmidt et al., 2006). Further, one cannot be sure, that the longest radius contains the most annual rings. This was the reason why two to four radii per disc were measured.

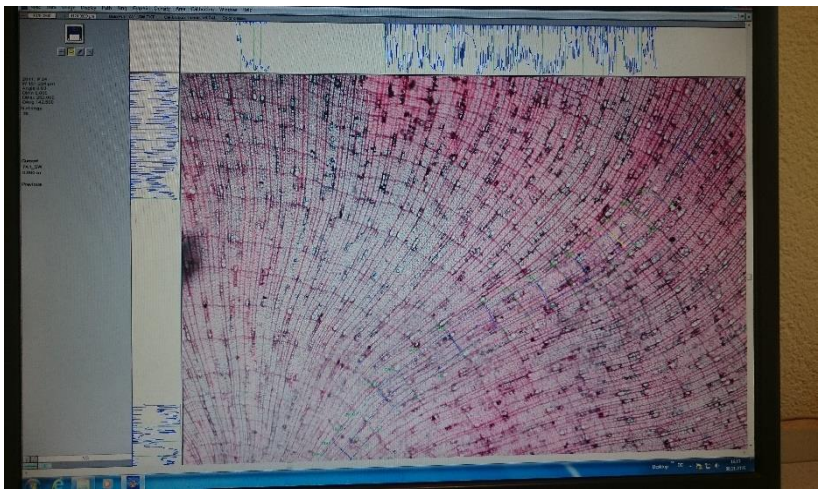

Figure 16: *Ring-width measurement with WinDENDRO.*

4.2.2.6. Cross-dating with TSAPWin

For the cross-dating a software called *TSAPWin* was used (Fig. 17). In a first step, the radii of one cross-section were cross-dated and averaged. Then the averages of two discs of one species were cross-dated. With these averages, the complete cross-dating was conducted. The cross-dating helped to get a relative age of the plants and to identify missing rings or rings, which have been incorrectly counted as rings. Additionally, changes in growth were visible and the years when these changes occurred.

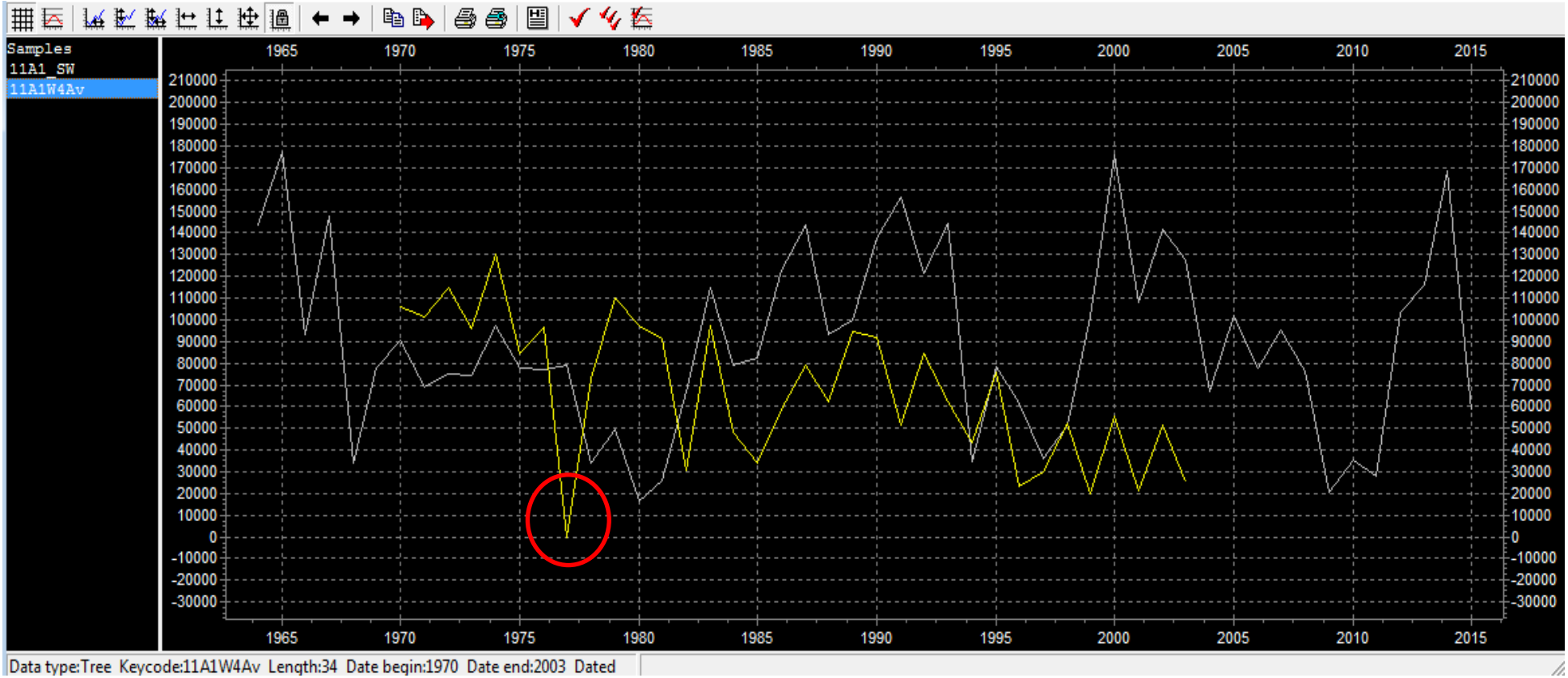

Figure 17: *Dead BN root (yellow) cross-dated with an "alive" BN (white). Red circle shows an inserted ring between 1976 and 1977.*

5. Results

5.1. Geochemistry and radiocarbon-dating

5.1.1. Soil description

The soils vary from moist mire-like to dry and sandy soils. The minimum thickness of 12 cm and the maximum thickness of 66 cm show a variation in the soil profiles. At each site 3–5 profiles have been sampled. For each site one reference profile was determined. The criteria for the reference profiles were that there are no external damages visible, that the profile is located at a higher elevation and far away from the coast (see chapter 4.1.1.).

5.1.1.1. Camp Site

The soil profiles 1, 2 and 4 at the *Camp Site* are moist and are with a depth around 15 cm less distinct (Fig. 18). The closer to the coast, the wetter the soils are. Profile 4 is located at a higher elevation and further away from the shore. Whereas profile 2 is directly at the shore and at the same height as the erosion line of the vegetation. Profile 1 lies between the soil profiles 2 and 4. The topsoils vary from 1–3 cm.

Figure 18: *Camp Site with profiles 1, 2 and 4. Profile 4 is used as the reference soil.*

5.1.1.2. Fox Beach

Profile 5 is above the marshy meadow, interspersed with stones, where profile 6 was sampled. The marbling in the fine soil of profile 5 indicates the high moisture in the soil. With a thickness of 66 cm, this profile is the thickest of all sampled soils. The rusty colour in profile 6 also suggests a mire-like soil. This profile reaches the bed rock at a depth of 27 cm. Both profiles are further away from the shore. Profiles 7 and 8 are sandy soils with a thickness of 15 cm and are coarser than profile 5 and 6. Site 8, which is the closest to the shore, containing a lot of sand and stones on its surface (Fig. 19).

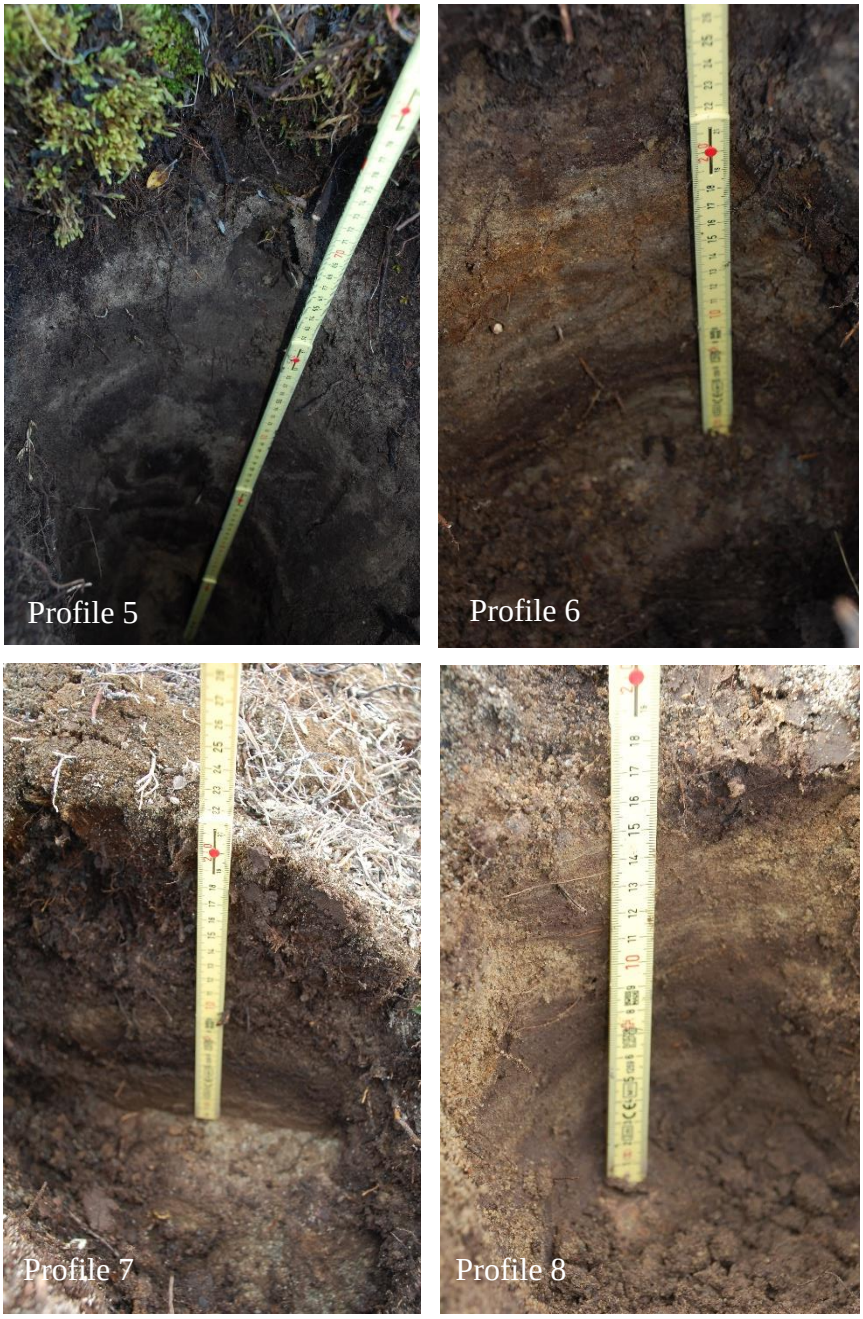

Figure 19: *Soil profiles 5-8 at Fox Beach, with profile 5 as the reference.*

5.1.1.3. Charlie

Profile 9 is placed next to the shoreline. The first 5 cm are fine (< 1 mm), laminated sand followed by an organic layer and transitions into a zone with glacial sediments before it reaches the bed rock in a depth of 20 cm. Its surface contains a lot of sand, stones and little shells. The organic topsoil of the profile 10 has a thickness of 5 cm. This profile is layered, laminated and contains a lot of sand with a small grain size (< 2 mm). Profile 11 has an organic topsoil of 12 cm. The mineral soil reaches a thickness of 20 cm. The lower half of the profile is laminated too. The reference profile 12 is 43 cm thick and has an organic topsoil of 7 cm. This soil shows a distinctive lamination and layering as well (Fig. 20).

Figure 20: *Site Charlie with the profiles 9-12. Profile 12 was determined as a reference.*

5.1.1.4. Delta

Profile 3 and 3* are at the same place and were sampled twice. 3 was sampled in Sumer 2015, due to a contamination of recent soil while sampling, the results of the radiocarbon-dating were distorted. Therefore, this site was sampled again (profile 3*, Summer 2016). They are located next to the coastline. Both profiles are dry and brittle. Between 4 and 11 cm there is very fine material. Then it changes into pebbles between 11 and 22 cm and after 22 cm into sandy material. The colour of the profile is greyish until this depth and changes to brown. This layer continues until a depth of 30 cm. After that, there is a mixture of stones and pebbles, which are oxidised at their bottom. The first 20 cm of site 13 are very sandy and the last 5 cm (20–25 cm) of the profile has a lot of small stones and few organic materials. The surface of those profiles is covered with a lot of sand and stones. Profile 14 gets to the bed rock in a depth of 16 cm. Those 16 cm soil are nicely layered. From 0–5 cm a sandy and organic layer can be observed. From 5–10 cm it looks like there is more organic material enclosed. After 10 cm the material gets very fine (Fig. 21).

Figure 21: *Profiles 3, 3*, 13, 14 and 15 at Delta, with site 15 as the reference.*

5.1.2. Loss on Ignition

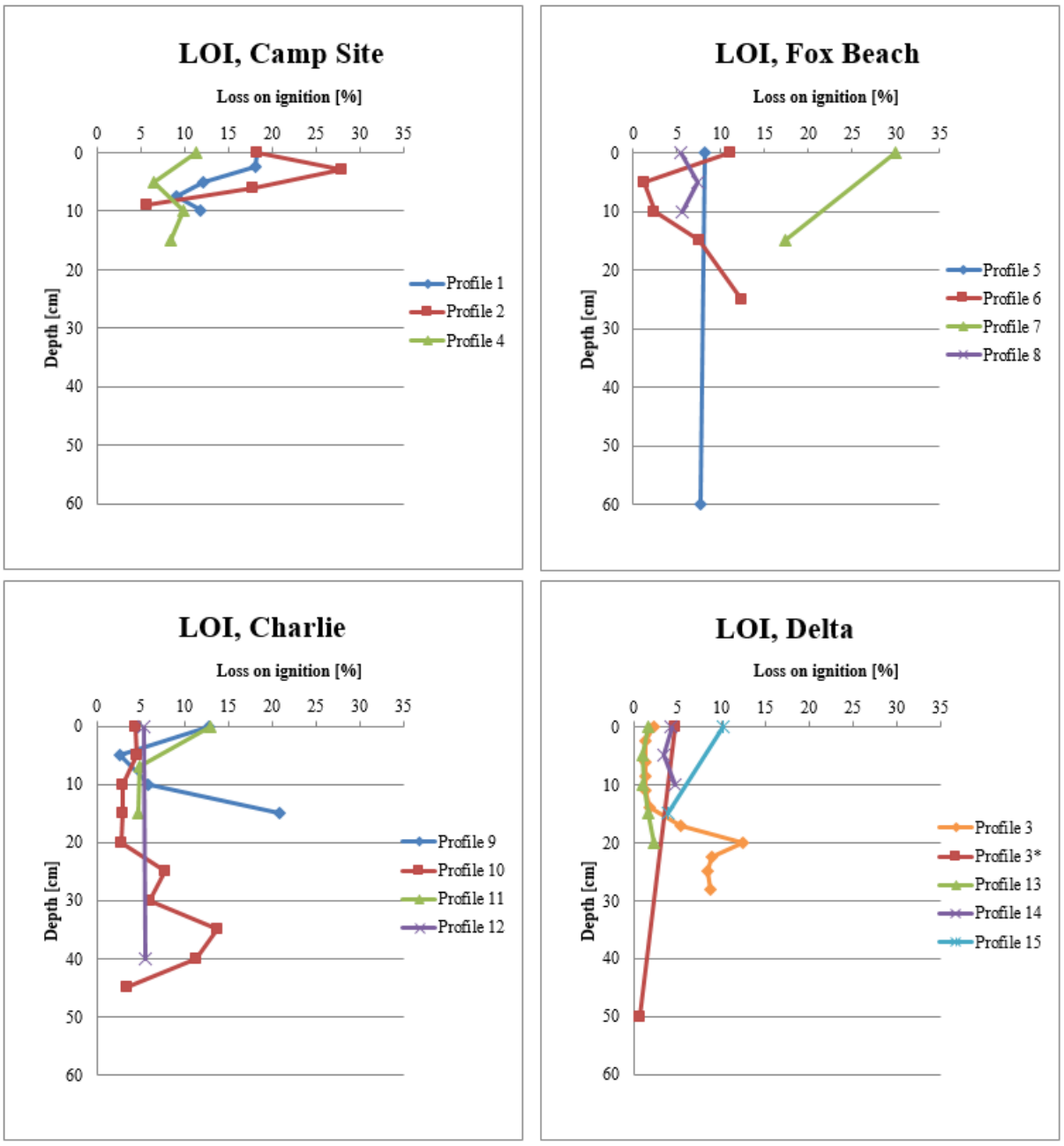

Figure 22: *Loss on ignition [%] at Camp Site, Fox Beach, Charlie and Delta. Profile 2, 8, 9, 3, 3* in the dead zone; Profile 7, 10, 13 in the affected zone; Profile 1, 6, 11, 14 in the transition zone; Profile 4, 5, 12, 15 in the reference zone.*

The LOI at Camp Site shows an increase until 2.5 cm for site 2. After that, the organic content decreases towards bed rock. Profile 1 and 4 show an opposite progression. After a decrease of organic content until 5 and 7.5 cm, it starts to increase until 10 cm. The LOI of profile 4 decreases again after 10 cm (Fig. 22).

Profile 8 at Fox Beach follows a similar pattern as profile 2 from Camp Site. Until 5 cm an enhancement of organic material can be observed and it is continuously reduced between 5 and

10 cm. Profile 6 acts in a similar way as Site 1. After a decrease of the LOI until 5 cm it increases until it reaches the bed rock. Profile 5 and 7 were only sampled at the top and the bottom of the profile. Therefore, variations in between cannot be seen (Fig. 22).

Charlie has a general lower LOI compared to Camp Site and Fox Beach. Profile 9 decreased from 13 to 3% within the first 5 cm and increases up to 21% at a depth of 15 cm. Site 10 shows a little decrease until 20 cm, followed by an increase to 14% at 35 cm. After that the organic content returns to a similar value as it is at the top of this profile. The LOI retreats from 13% to 5% at a depth of 7 cm and remains there. Profile 12 has also been sampled at the top and bottom (Fig. 22).

Because profile 3 at Delta was already sampled and analysed every 3 cm. Site 3* was only sampled at the top and the bottom. Even though these profiles were located extremely close to each other, they show differences in the LOI. Profile 3 begins with little organic content and starts to enhance its concentration down to 20 cm from 2% to 12%, followed by a slight decrease. The LOI of 3* is very low. It starts at 5% and ends at 0.7% in a depth of 50 cm. At profile 15 a decrease from 10% to 4% can be observed within 15 cm. This profile was also sampled at the top and the bottom (Fig. 22).

LOI shows the quantity of the organic material, the results of the Si-concentration (Fig. 24) from the XRF analysis presents the amount of inorganic material. Therefore, LOI and Si should correlate together. The higher the organic material the lower Si-concentration.

5.1.3. XRF

5.1.3.1. Sodium

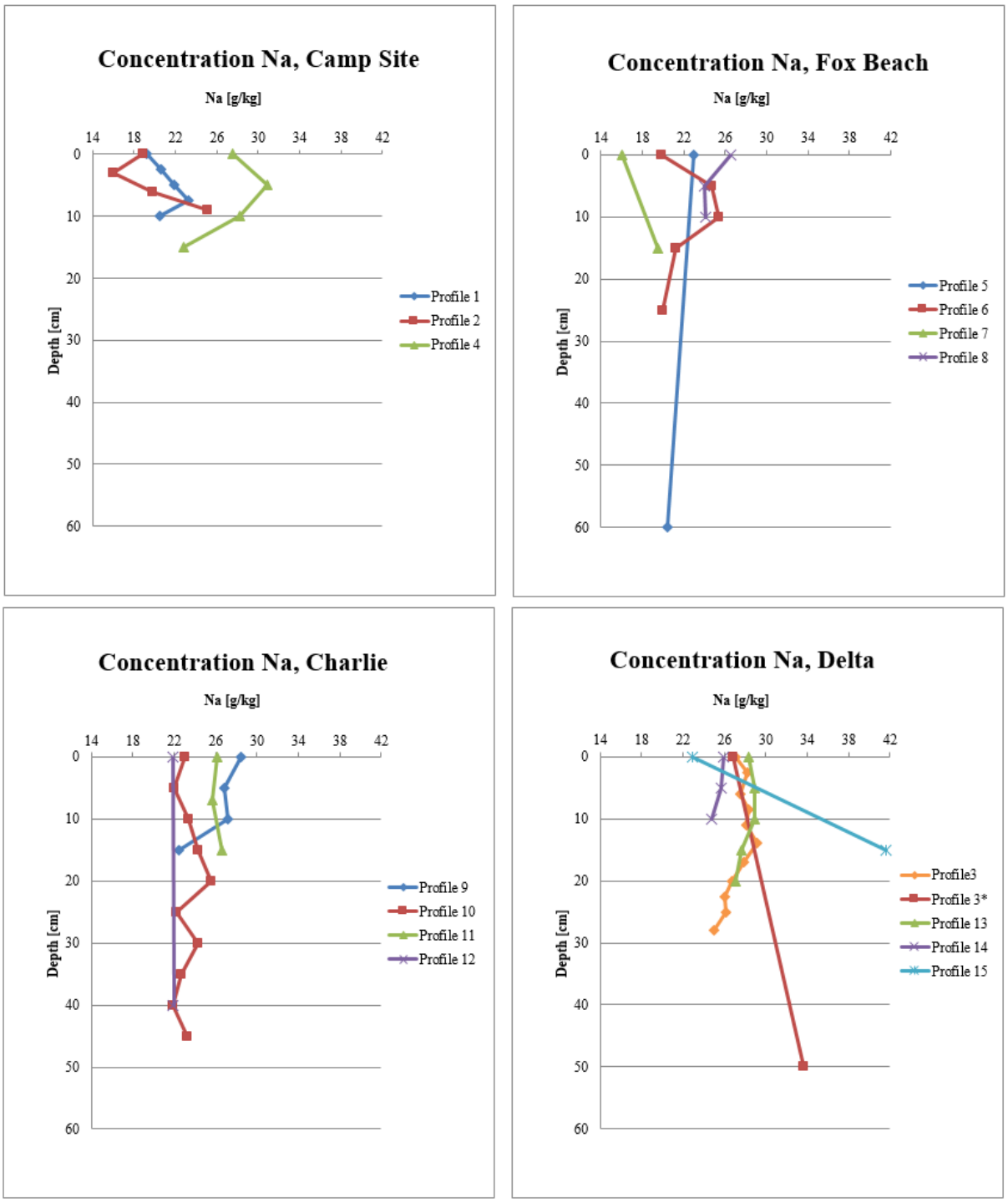

Figure 23: *Na-concentration at Camp Site, Fox Beach, Charlie and Delta. Profile 2, 8, 9, 3, 3* in the dead zone; Profile 7, 10, 13 in the affected zone; Profile 1, 6, 11, 14 in the transition zone; Profile 4, 5, 12, 15 in the reference zone.*

Compared to profile 2, profile 1 and 4 at Camp Site increase in their Na-concentration within the first 5 cm and 7.5 cm. After this increase, a decrease can be observed in both profiles.

However, profile 2 shows a decrease from 18 g kg^{-1} to 16 g kg^{-1} within the first 3 cm. The increase of Na ends at 9 cm with a maximum of 25 g kg^{-1} (Fig. 23).

Profile 5 and 7 at Fox Beach are not very significant, because it cannot be determined if there is a decrease or increase in the Na-concentration in the first few cm. After an increase of the concentration until 10 cm at site 6, it starts to retreat from 25 g kg^{-1} to 20 g kg^{-1}. Profile 8 shows a decrease of the Na-concentration until 5 cm depth and stagnates until 10 cm (Fig. 23).

The concentration of Na remains between 22 g kg^{-1} and 29 g kg^{-1} at Charlie. Profile 9 decreases slowly until 10 cm and then start to decrease rapidly until 15 cm. Profile 10 and 11 show little variations (Fig. 23).

Profile 3, 13 and 14 at Delta are more or less steady along the profile with a slight decrease. The most significant difference, with 20 g kg^{-1} more Na within 15 cm, can be observed in profile 15 (Fig. 23).

5.1.3.2. Silicon

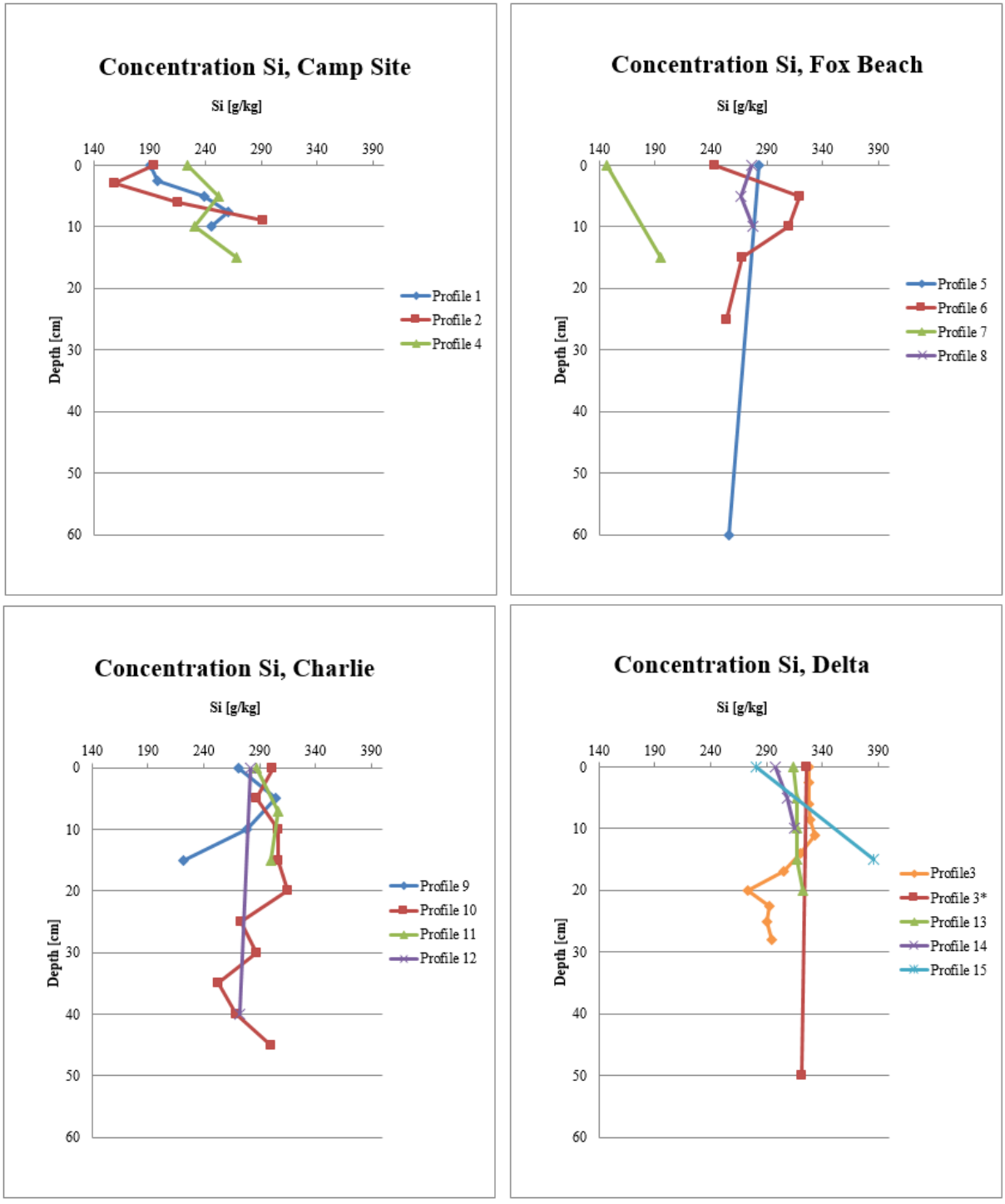

Figure 24: *Si-concentration at Camp Site, Fox Beach, Charlie and Delta. Profile 2, 8, 9, 3, 3* in the dead zone; Profile 7, 10, 13 in the affected zone; Profile 1, 6, 11, 14 in the transition zone; Site 4, 5, 12, 15 in the reference zone.*

At Camp Site, the Si-concentration in profile 1 and 4 increases until 7.5 cm respectively 5 cm. After this increase both concentrations decrease until 10 cm and profile 4 increases again until the bed rock. Profile 2 starts at a Si-concentration of 194 g kg^{-1}, which is reduced within the

first 3 cm to 159 g kg^{-1}. Until 9 cm it increases rapidly to a concentration of 292 g kg^{-1} (Fig. 24).

Profile 6 at Fox Beach shows large variations. Within the first 5 cm it increases rapidly from 244 g kg^{-1} to 319 g kg^{-1}. This increase is followed by a decrease which flattens between 15 cm and 25 cm. Profile 8 stable with a little decrease at 5 cm depth and a small increase towards 10 cm (Fig. 24).

Profile 9 at Charlie decreases to 222 g kg^{-1} after an increase from 271 g kg^{-1} to 304 g kg^{-1} within the first 5 cm. Significant changes in profile 10 are measured after 20 cm depth. The Si-concentration decreases from 315 g kg^{-1} to 254 g kg^{-1} until 35 cm and goes up to 300 g kg^{-1} at a depth of 45 cm (Fig. 24).

At Delta, profile 3 presents a stable Si-concentration until 11 cm. Between 11 cm and 20 cm a decrease can be observed. After a little increase, the Si-concentration stabilizes. Profile 14 shows a little increase along the whole profile. The concentration in profile 15 was only measured at two points. However, in this case an increase from 281 g kg^{-1} to 386 g kg^{-1} is visible (Fig. 24).

5.1.3.3. (Ca+K)/Ti

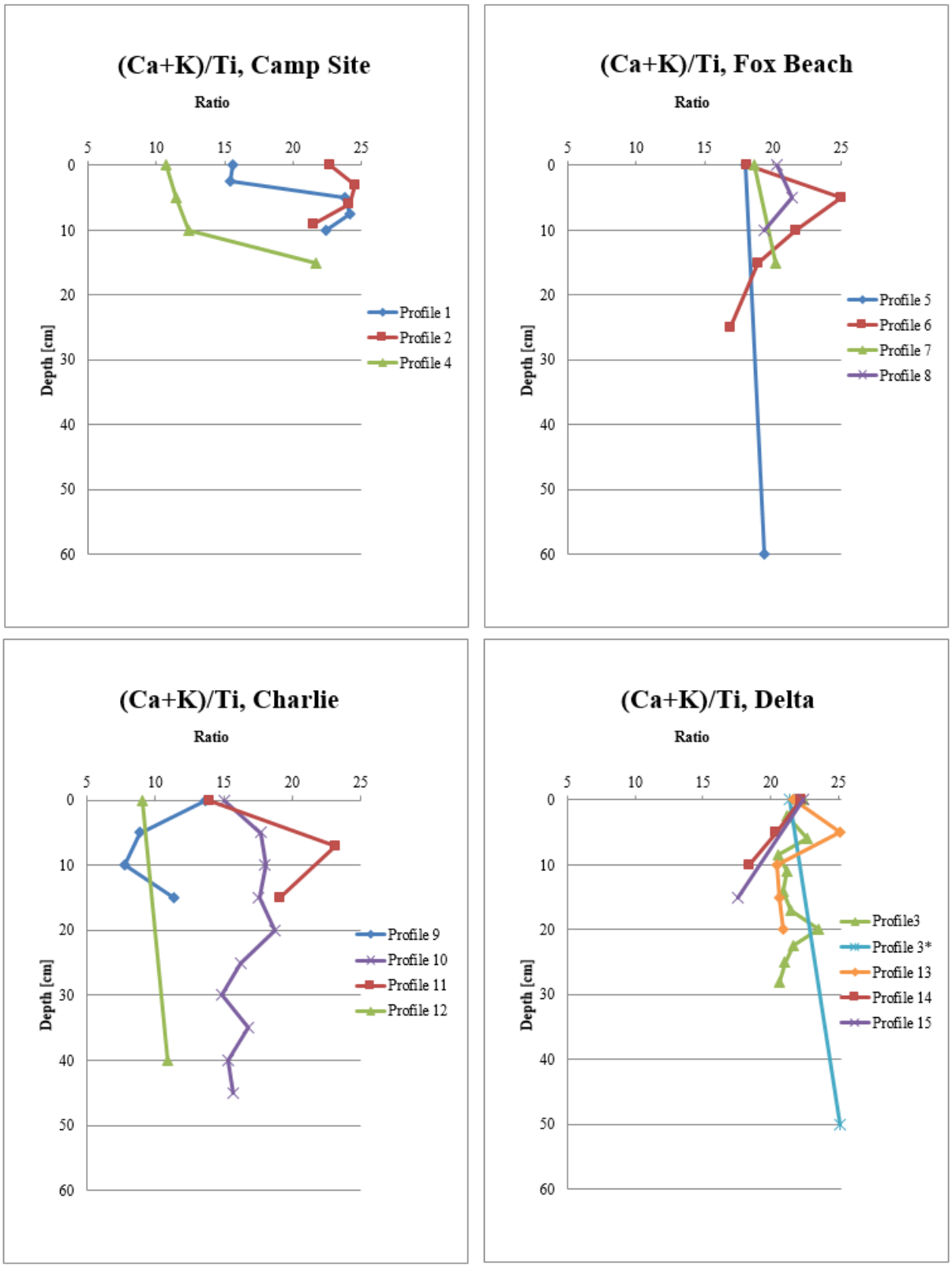

Figure 25: *Calcium-potassium Titanium ratio at Camp Site, Fox Beach, Charlie and Delta. Profile 2, 8, 9, 3, 3* in the dead zone; Profile 7, 10, 13 in the affected zone; Profile 1, 6, 11, 14 in the transition zone; Profile 4, 5, 12, 15 in the reference zone.*

Profile 4 at Camp Site shows a nice trend of the (Ca+K)/Ti ratio. Within the first 10 cm the ratio is low and decreases until 15 cm. The upper soil is usually more weathered and therefore presents a lower ratio. Profile 2 shows the least significant weathering of all profiles at Camp Site.

At Fox Beach, mire-like profile 6 illustrates a nice pathway course of the ratio as well. It goes from more to less weathered within the first 5 cm. The increase towards bottom could be influenced by the soil moisture.

Profile 9 at Charlie is close to the erosion line. Tsunamis eroded the upper part of the soil and therefore the first 5 cm are less weathered. Less variations are observed in profile 10.

The profiles at Delta seem to be not much weathered due to their ratio. Profile 14 and 15 are not located in the dead zone. Nevertheless, they show a similar trend as profile 9 at Charlie. The soils at Delta are dry and sandy and exposed to wind. It is possible that these profiles are influenced by the wind that erodes the first cm of soil and therefore less weathered material can be found at the surface.

5.1.3.4. K/Rb

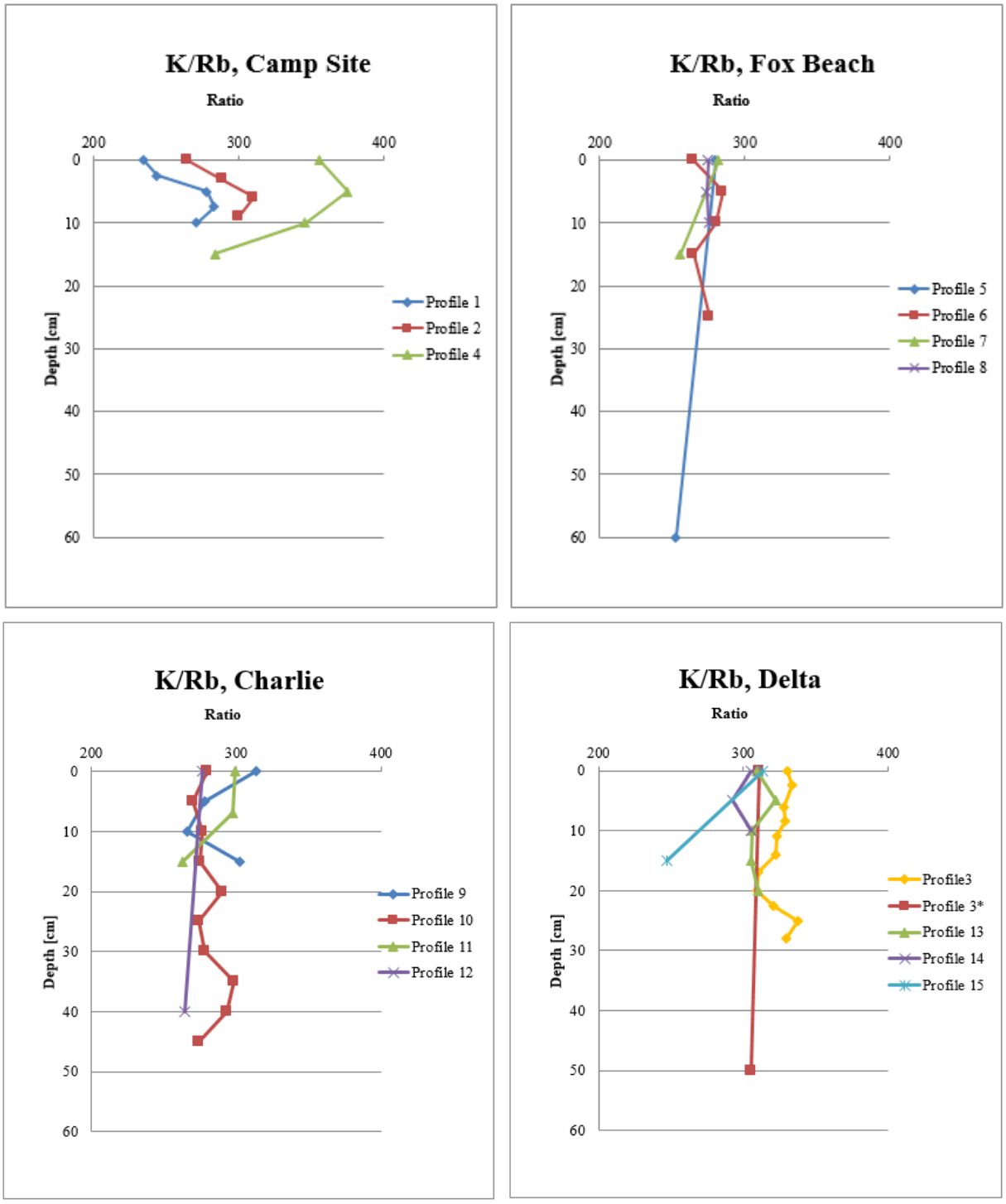

Figure 26: *Potassium-rubidium ratio at Camp Site, Fox Beach, Charlie and Delta. Profile 2, 8, 9, 3, 3* in the dead zone; Profile 7, 10, 13 in the affected zone; Profile 1, 6, 11, 14 in the transition zone; Profile 4, 5, 12, 15 in the reference zone.*

Profile 1, 2 and 4 at Camp Site and profile 15 at Delta show big variations in the K/Rb ratio. Therefore, these profiles are affected by aeolian dust. The other profiles do not show big variations and hence the soil formation was not stronlgy influenced by aeolian dust and the soil minerals seems to be of the same material (Fig. 26).

5.1.4. pH

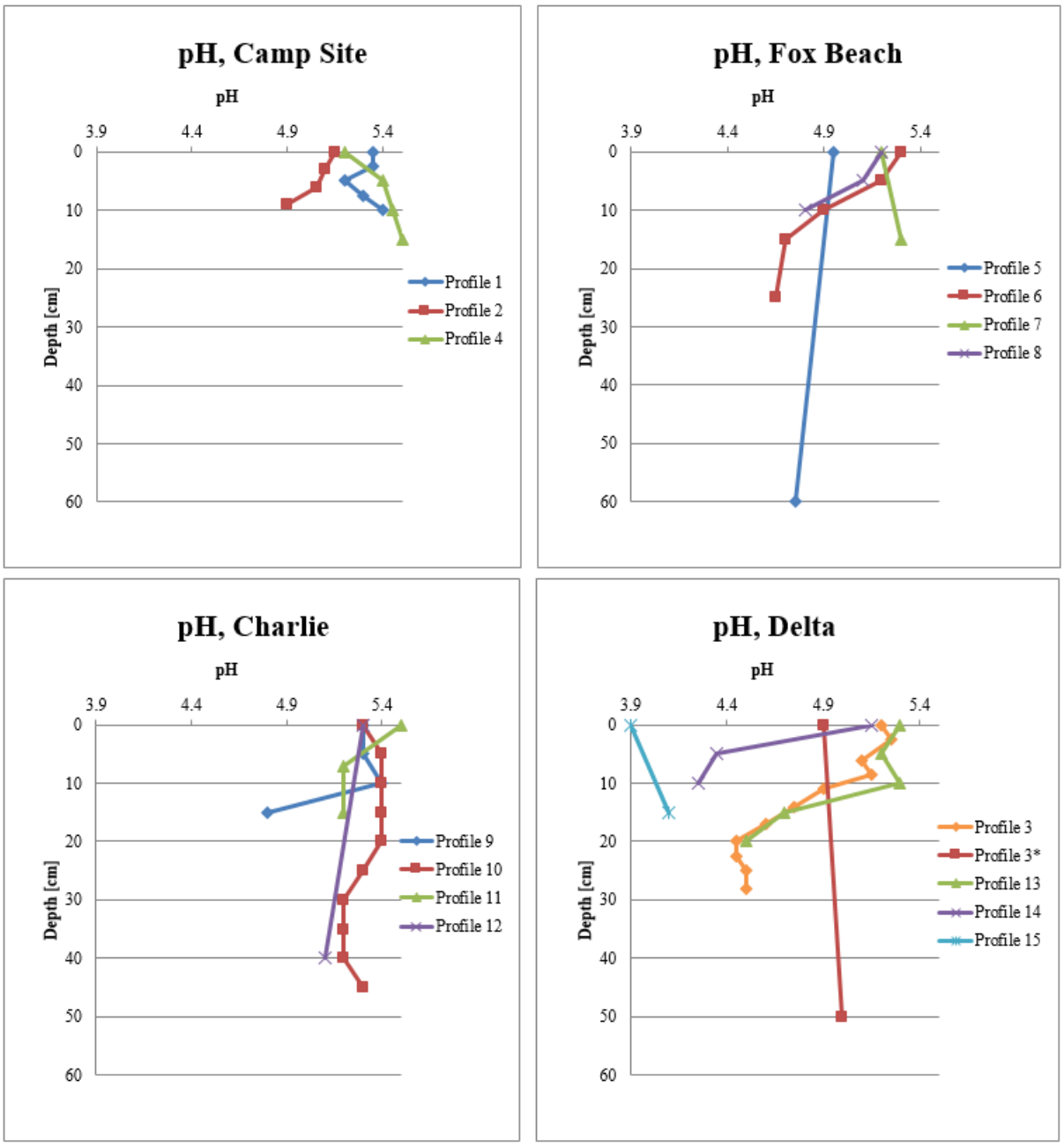

Figure 27: *pH-values at Camp Site, Fox Beach, Charlie and Delta. Profile 2, 8, 9, 3, 3* in the dead zone; Profile 7, 10, 13 in the affected zone; Profile 1, 6, 11, 14 in the transition zone; Profile 4, 5, 12, 15 in the reference zone.*

The pH-values at Camp Site range between 4,9 and 5,5. A decrease between 2.5 cm and 5 cm can be observed in profile 1. Between 5 cm and 10 cm the pH increases up to 5,5. Profile 2

starts with a pH of 5,15 and reaches its minimum at 9 cm with 4,9. Profile 4 follows an opposite trend compared to the other two profiles. The pH-value at this profile increases slightly towards bed rock from 5,2 to 5,5 (Fig. 27).

Profile 6 and 8 at Fox Beach show a bigger decrease in their pH-value, whereas the pH-value of profile 5 shows a continuous negative trend towards bed rock. The pH of profile 7 shows a little increase down to 15 cm (Fig. 27).

All profiles at Charlie, except profile 9 show little variations in their pH. They are all situated between 5,1 and 5,4. The pH at profile 9 starts to decrase in a depth of 10 cm down to 15 cm from 5,4 to 4,8 (Fig. 27).

With a range of a pH-value range of 3.9 to 5.25, the biggest variations can be observed at site Delta. Profile 3 and 13 behave in a similar way. In the upper 10 cm, the pH changes little but decreases remarkably after 10 cm. Within the first 5 cm, profile 14 shows a decrease in its pH from 5.15 down to 4.35. It returns to a pH of 4.5 at 10 cm depth. Profile 15 is the only profile with a pH-value below 4. It starts with 3.9 and increases up to 4.1 within 15 cm. This soil is therefore the most acid profile out of all samples (Fig. 27).

5.1.5. C/N

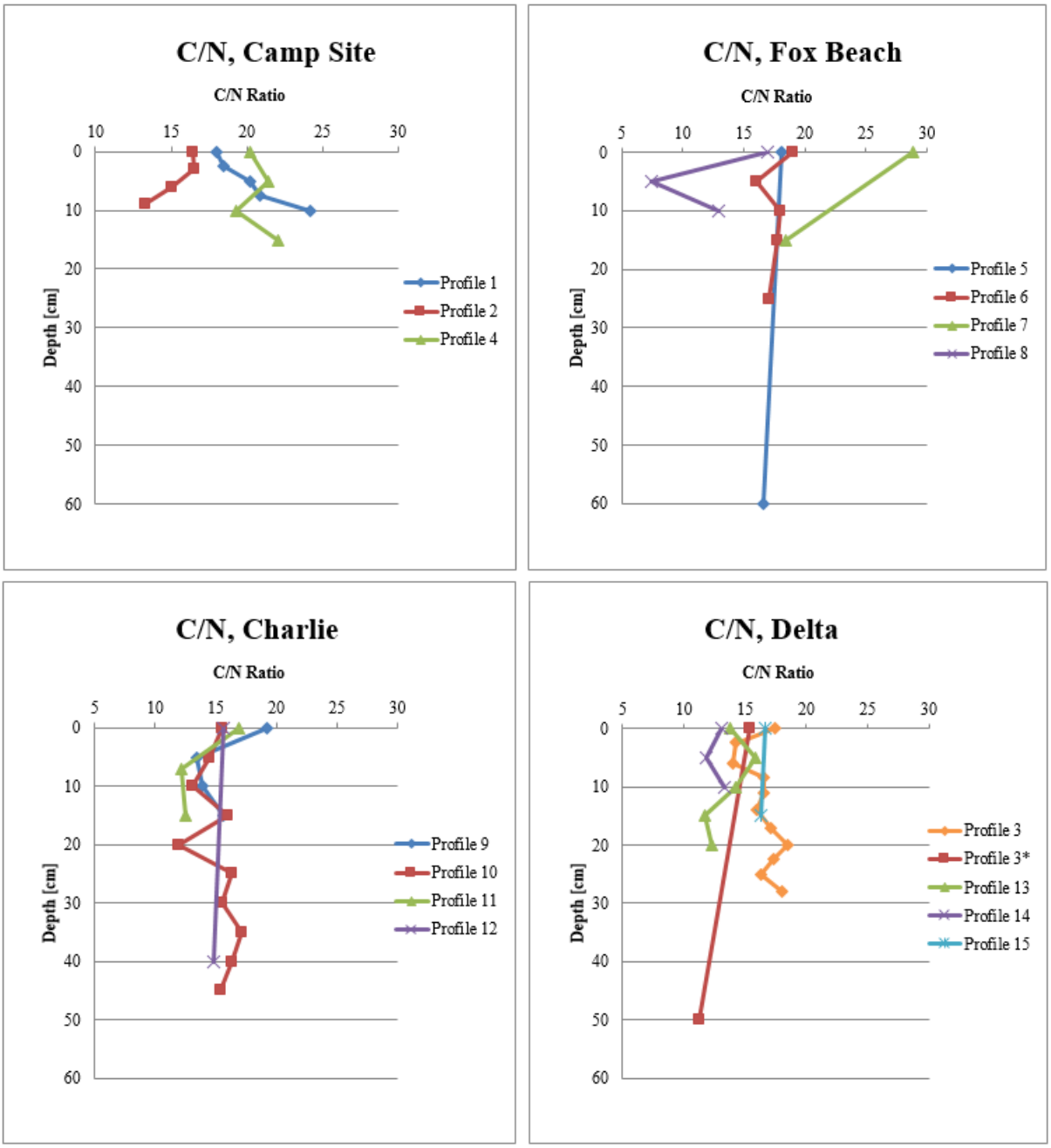

Figure 28: *Carbon Nitrogen ratio at Camp Site, Fox Beach, Charlie and Delta. Profile 2, 8, 9, 3, 3* in the dead zone; Profile 7, 10, 13 in the affected zone; Profile 1, 6, 11, 14 in the transition zone; Profile 4, 5, 12, 15 in the reference zone.*

The C/N ratio at profile 1 at Camp Site grows continuously 18 to 24. Profile 2 shows a small decrease. Alternations between increase and decrease are detected at profile 4 (Fig. 28).

Profile 5 and 6 at Fox Beach do not show large variations, except a slight decrease at 5 cm in profile 6. A general decrease can be seen in profile 7. Profile 8 halves its C/N ratio towards 5 cm and increases again until 10 cm (Fig. 28).

At Charlie profile 9, 10 and 11 show similar C/N ratios until 10 cm, whereby profile 11 stays stable after 7.5 cm. Profile 9 and 10 increases after 10 cm until 15 cm. After that, the C/N ratio returns to 12 at 20 cm depth and increases again to 16 at 25 cm. A stabilization is visible between 25 cm and 45 cm (Fig. 28).

Profile 3 at Delta starts with a decrease and reaches the minimum ratio of 14 at the depth of 6 cm. The maximum C/N ratio of 18 is located at 20 cm. A slight increase in the beginning is measured at profile 13. After 5 cm, the C/N ratio shrinks to 12 at 15 cm and stays near this value at a depth of 20 cm. Profile 14 show a little decrease at 5 cm but returns to the same ratio as in the beginning (Fig. 28).

5.1.6. Radiocarbon

Profile	Depth [cm]	Prep. Technique	Material	C14 age [BP]	±1σ	1-sigma [cal AD]	1-sigma [cal BP]	2-sigma [cal BP]
2	3	AAA	organic matter	108	23	1694-1918	257-33	268-20
	9	AAA	organic matter	-580	23	2003-2004	(-52)-(-54)	(-6)-(-55)
3	0	H2O2	soil	1643	26	382-427	1569-1524	1613-1419
	23	H2O2	soil	597	25	1310-1400	640-551	652-542
	23	AAA	organic matter	18	23	1893-1906	58-44	245-35
5	63	H2O2	soil	8559	31	7597-7574	9546-9523	9550-9494
6	0	AAA	organic matter	-489	22	2005-2007	-55-(-57)	-6-(-58)
	25	AAA	organic matter	901	23	1047-1169	904-782	910-743
7	2	AAA	organic matter	-803	22	1997-1998	-47-(-48)	-7-(-49)
	12	AAA	organic matter	-244	22	1955-1956	-5-(-6)	-5-(-7)
13	23	H2O2	soil	7411	33	6335-6236	8304-8185	8329-8176
15	17	AAA	organic matter	729	22	1267-1284	684-667	693-659

Table 1: *Radiocarbon-dating with the ^{14}C ages and the calibrated ages [AD] and [BP] and the pre-treatment of the materials of the Camp Site, Fox Beach, Charlie and Delta. Profile 2 and 3 in the dead zone; profile 7 and 13 in the affected zone; profile 6 in the transition zone; profile 5 and 15 in the reference zone.*

To calibrate the ^{14}C ages the IntCal13 curve was used by the online Oxcal calibration tool (Reimer et al., 2013).

The expected stratigraphy would be young over old. The oldest sample was found in profile 5 at a depth between 61–66 cm with a calibrated (cal.) age BP between 9546–9523. This is the last sampled horizon in this profile and the deepest sample of all soils. Another old sample was measured at profile 13 between 20–25 cm. With an age cal. BP of 8304–8185 it is the second

oldest sample. A special chronology shows profile 3. The oldest sample in this profile is located at the very top and the youngest at the bottom. The other samples do not show the expected chronology (Table 1).

Figure 29 shows an overview of the dated samples. Since site Delta is the farthest way from the glacier, it is expected to get the oldest age here, because it was first deglaciated. Thus, the youngest samples should be found at Fox Beach. However, the oldest sample was detected at Fox Beach.

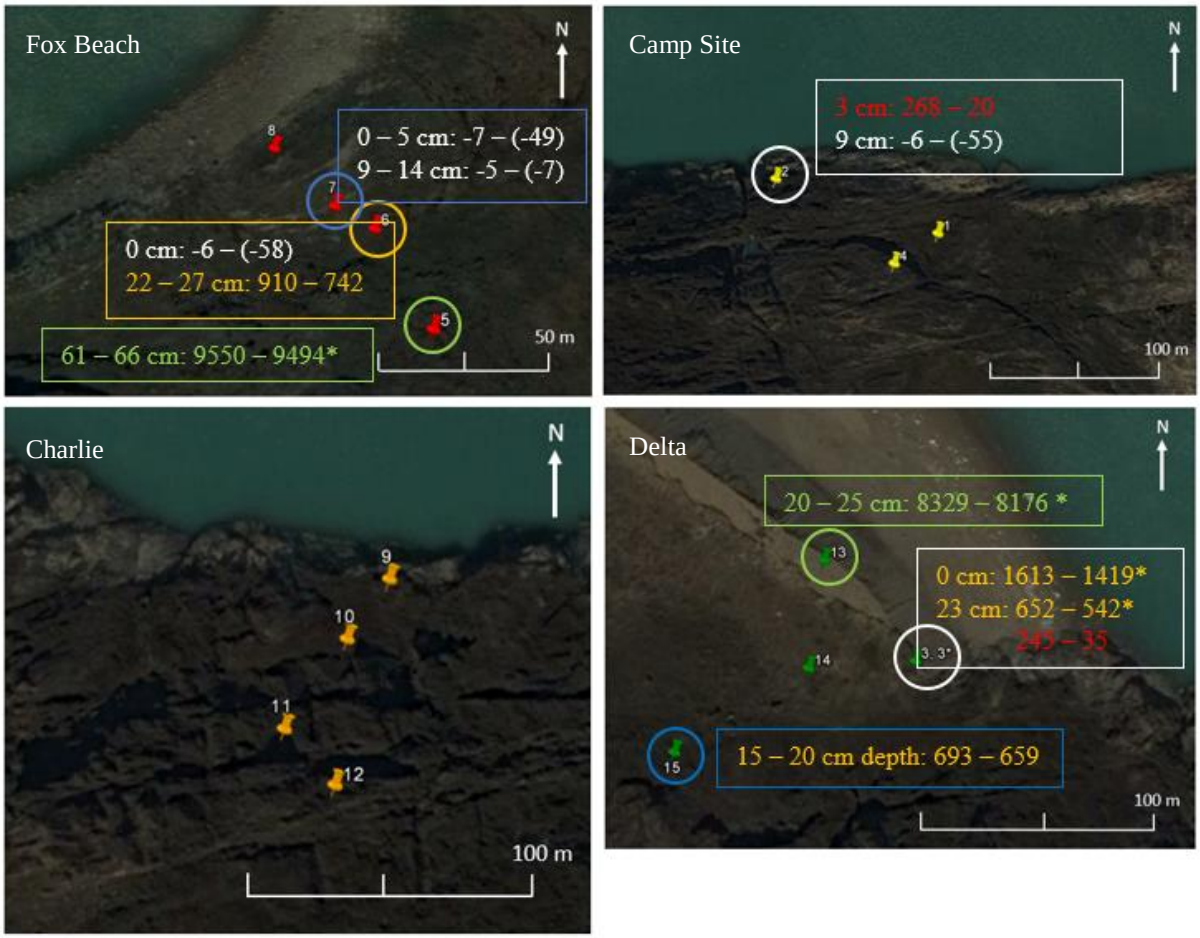

Figure 29: *Map with ^{14}C ages cal. BP: Fox Beach is the nearest to the glacier, then Camp Site, then Charlie and Delta is the farthest located site. The cal. BP ages with * are pretreated with H_2O_2; the others with AAA-technique. White numbers: modern age; red numbers: young age; orange numbers: middle age; green numbers: old age.*

Figure 30 shows a chronology in depth of the cal. BP ^{14}C ages. The samples pretreated with the AAA-technique (Fig. 30 a)) present recent ages, not older than 800 cal. BP. Ages up to approximately 10 ka were measured in a depth of 65 cm (Fig. 30 b)). This sample was pretreated with H_2O_2. The age should increase with depth. This is the case in Figure 30 a) and 30 b), whereas much modern ages were dated at the surface, in 10 cm, 15 cm depth and younger age in 25 cm depth (Fig. 30 a)).

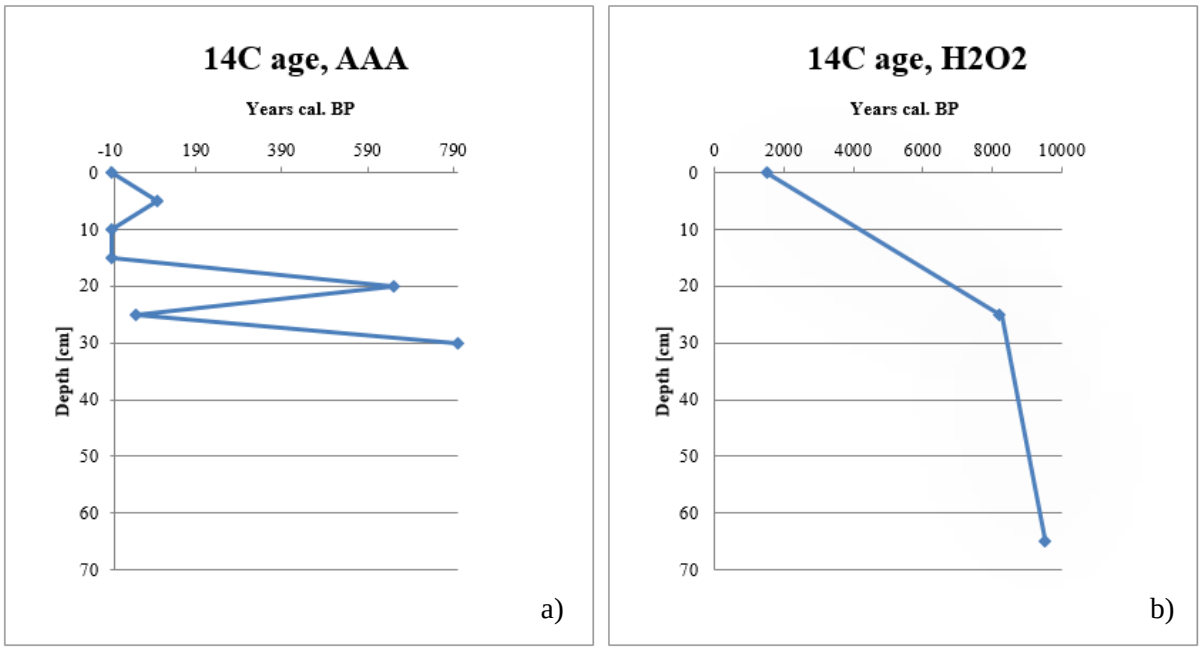

Figure 30: *^{14}C ages cal. BP, a) samples pretreated with the AAA-technique and b) samples pretreated with H_2O_2. For this illustration, the average age was taken from the 2σ range.*

5.2. Dendrochronology

5.2.1. Cross-dating

Table 2 shows all collected dwarf shrubs with their relative age which are counted annuals rings (length), when they started to grow and when they died.

Site	Betula Nana	Length	Date begin	Date end	Salix Arctica	Length	Date begin	Date end
Fox Beach	5A	68	1948	2015	5B	83	1933	2015
	6A	49	1967	2015	6B	49	1967	2015
	7A	51	1965	2015	7B	13	2003	2015
	8A	42	1971	2012	8B	33	1969	2001
Charlie	9A	48	1953	2000	9B	51	1953	2003
	10A	21	1995	2015	10B	86	1930	2015
	11A	52	1964	2015	-	-	-	-
	11AWF	33	1968	2000	-	-	-	-
	12A	31	1985	2015	12B	53	1963	2015
Delta	-	-	-	-	13B	32	1984	2015
	14A	37	1979	2015	14B	77	1939	2015
	15A	19	1997	2015	15B	62	1954	2015

Table 2: *BN and SA dwarf shrubs at Fox Beach, Charlie and Delta with their relative ages and their date of death. Reference plants in blue and plants in the dead zone in orange. The transition zone and the affected zone is in white.*

The oldest plant is a SA with 86 counted annual rings. The oldest BN has as a relative age of 68 years. With an average age of 54 years the SA is 13 years older than the BN. The plants 8B, 9A, 9B and 11AWF (exposed root) died between 2000 and 2003. 8A died later in 2012, whereby 13B was still alive at the time of sampling. Camp Site is missing, because it was not sampled, either in 2015 or 2016. Furthermore, the plants 11B and 13A could not be sampled, because there were no dwarf shrubs available at these spots.

In the figures 31 and 32 the SA (12B) is used as a reference plant. This plant was chosen as reference for the figures 31 and 32, because this dwarf shrub showed the most constant growth compared to the other reference plants from the other three sites. This SA has grown far away from the coast and at a higher elevation (30m a.s.l.). Therefore, this plant has not been affected by tsunamis at all. For the visualization of the results, only the most informative data have been used. This means that there have been dwarf shrubs, which were too young and therefore not significant enough. Additionally, the graphic would be hard to read, if there were too many data shown.

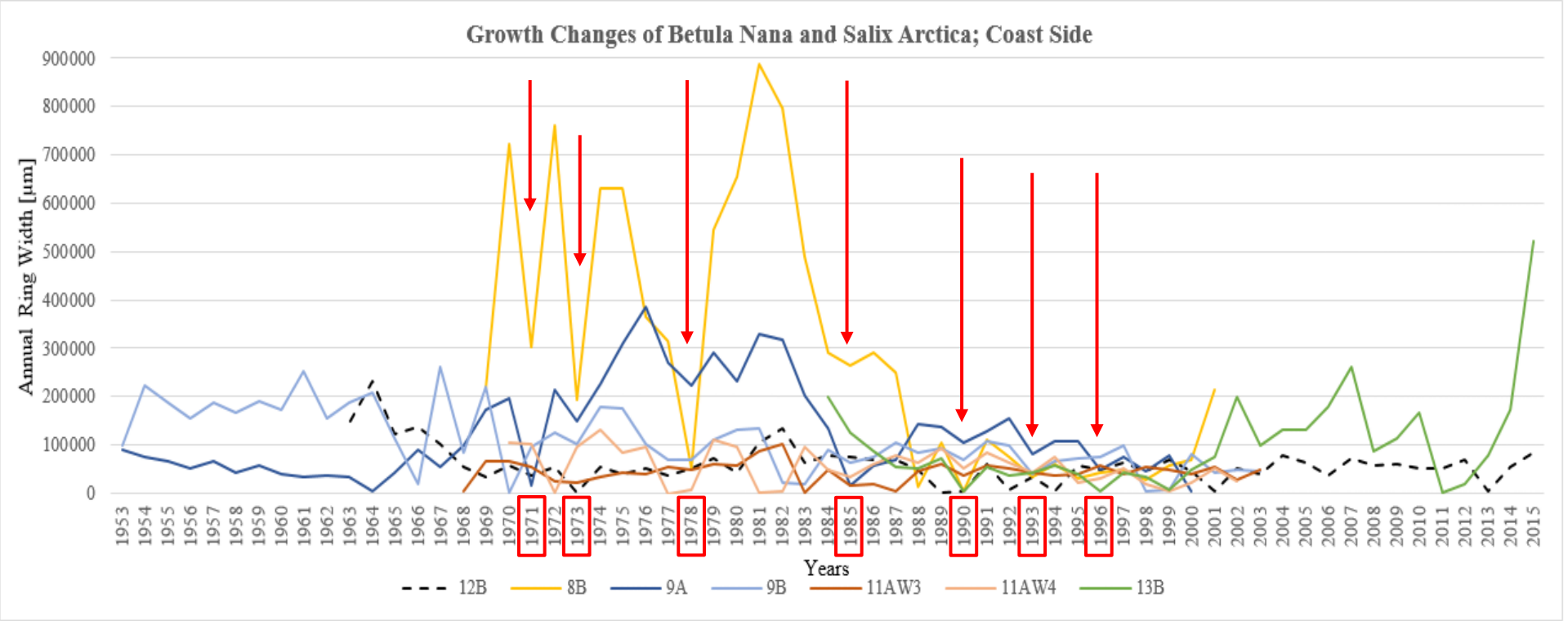

Figure 31: *Annual ring widths of the BN (9A, 11AW3, 11AW4) and the SA (12B = reference plant, 8B, 9B, 13B) at the dead zone. Red arrows and boxes show the decreases in ring width at 1971,1973,1978,1985, 1990, 1993 and 1996.*

Figure 31 shows the growth reaction of the dwarf shrubs in the dead zone. The red boxes mark the years 1971, 1973, 1978, 1985, 1990, 1993 and 1996. These years mirror local minima in the width of the annual rings of all plants, which is highlighted with arrows. It is important to say, that this is not an absolute chronology. Consequently, such changes in growth could be shifted by one or two years. Particularly the year 1985 illustrates a big decrease in their annual ring width, especially for 8B and 9A. Expect the dead SA (8B) shows already a first reduction in the ring width in 1984. Furthermore, little decreases in the annual ring width can be observed in 1990, 1993 and 1996. Even though the reduction in the annual rings in these years are not very clear, this decrease can be observed in all the plants, except in 12B (reference plant). Additionally, the dwarf shrubs in the transition zone (Fig. 32) do not show the same reactions as the plants in the dead zone. In the year 2000 the first plants began to die and further plants died between 2000 and 2003 (Fig. 31).

Further, SA 13B (Fig. 32) was with 22m a.s.l. at the highest elevation of all plants within the dead zone. It seems as if this dwarf shrub recovers after 2000 and shows later decreases in its growth in the years 2008 and 2011. It is uncertain, if this correlates with the tsunami-events, because some plants in the transition zone (Fig. 32) decrease in their growth as well (2008 ± 1 year and 2012 ± 1 year).

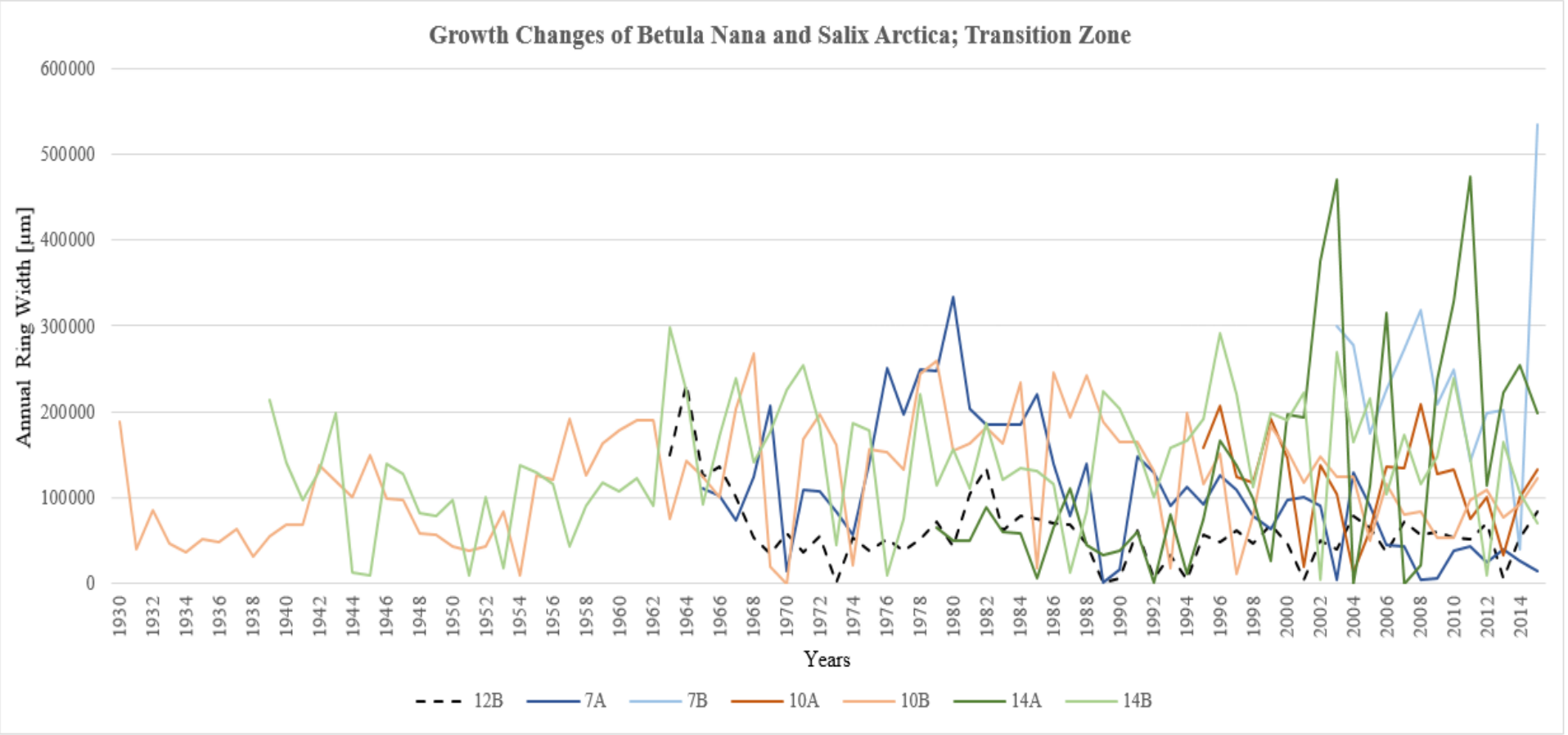

Figure 32: *Annual ring widths of the BN (7A, 10A, 14A) and SA (12B, 7B, 10B, 14B) at the transition zone.*

6. Discussion

6.1. Geochemistry

The most important profiles for the discussion are those, which are the closest to the coast. Profile 2, 3, 3*, 8 and 9 will therefore be compared with the other profiles at the same site. For certain points, it makes more sense to zoom out and do a cross-comparison between the four sites, with a focus on the profiles next to the shore.

In general it can be assumed that the pH-value increases after a tsunami-event and so do the Na, K, Ca, Mn and Fe contents (McLeod et al., 2010). The pH-value only slightly increases in all profiles at the shore within the first cm. The Na content (Fig. 23) does also increase in the upper soil, except for profile 3. Since this profile is located at an elevation of 20 m a.s.l., it is possible that this profile has not been hit by a tsunami for a longer time. Further the amount of K (Appendix II 4) is not increasing in profile 8 and 9, but increases in profile 2 and is more or less stable in profile 3 until 15 cm and decreasing after 15 cm. The content of Ca (Appendix II 3) increases like McLeod et al. (2010) describe, except for profile 3 that shows higher values not until 10 cm depth. In profile 2 and 3 Fe and Mn content incease (Appendix II 2 and 5), whereas these values decrease in profile 8 and 9 within the upper centimeter. These Elements have been leached in deeper into the soil, probably because these two profiles are at a lower elevation than profiles 2 and 3 and therefore got hitten by a tsunamis more often, resulting in leaching of these elements.

6.1.1. Camp Site

Figure 22 shows the LOI of the Camp Site. The higher the LOI is, the more organic material was burnt during the 6 hours at 550°C in the oven. Profile 2 is the only profile at Camp Site that presents a decrease from 2.5 cm up to the surface. This indicates that the organic content gets smaller toward the soil surface. The Si-concentration in figure 24 confirms the decrease of organic material. In profile 2 an increase of Si can be observed from 2.5 cm to 0 cm. Since profile 2 is next to the shore, it gets covered with siliceous sand and therefore the concentration of Si increases towards the top of the profile. Compared to profile 2, profile 1 and 4 show inverse values in the Si-concentration and in the LOI. Furthermore, an accumulation of Na (Fig. 23) is measured in profile 2 within the first 2.5 cm. This can be explained by the tsunamis, which bring seawater to the top of the soil. Since the average precipitation of 436mm per year in the Eqip Sermia area is low, displacements of the elements in the soil happens very slowly

(Hansen et al., 2006). Nonetheless, profile 2 shows a clear dislocation of Na, Si, Al from 2.5 cm down to 9 cm, where the highest concentration of these elements can be found (Fig. 23, 24, Appendix II 1)).

6.1.2. Fox Beach

The LOI at Fox Beach (Fig. 22) illustrates trends related to the LOI at Camp Site. Profile 8 in the dead zone decreases in its organic material from 5 cm to the surface. Even though it is not as distinct as in profile 2, a difference can be observed between profile 8 and the other profiles at Fox Beach. This difference between profile 2 and 8 might be caused by the soil type. Profile 2 has more mire-like attributes and profile 8 contains a lot of sand and shows lower humidity than profile 2. Therefore, profile 8 contains less organic material than profile 2. This is also visible by looking at the Si-concentrations (Fig. 24). Profile 8 increases just slightly in its Si-concentration from 5 cm to 0 cm. The little variance within profile 8 reflects the sandy type of the soil containing less organic material. The Na-concentration in profile 8 (Fig. 23) indicates a similar trend as profile 2. An increase of Na towards the surface indicates changes in its environment, assumingly due to tsunami-events. The other elements Al and Fe (Appendix II 1 and 2) do not show any big fluctuations, due to the lower mobility (Boxleitner et al., 2017).

6.1.3. Charlie

Profile 9 start with an increase of the LOI from 5 cm to 0 cm (Fig. 22). The highest content of organic material could be measured at 15 cm. Even though profile 9 behaves differently compared to the other profile at Charlie, it does not follow the same trend as profile 2 and 8. It rather shows an inverse way, which was not expected. The organic layer at 15 cm can be observed in the picture of the profile (Fig. 20). The LOI can be verified by the Si-concentration (Fig. 24) at profile 9. While the LOI is decreasing at 5 cm, the Si is increasing and vice versa at 15 cm. A plausible explanation for the inverse behaviour of profile 9 compared to profile 2 and 8 could not be found. The Na-concentration (Fig. 23) increases slightly from 5 cm to 0 cm at profile 9. Compared to profile 10 to 12 it does not seem to be a significant increase. Since the soils are influenced by the sea air, which contains Na too, it could be accumulated by air instead of tsunami-events. Profile 9 is not outstanding comparing the Al-concentration (Appendix II 1) to the other profiles at Charlie. It is a relatively homogenous in its distribution of Al. With a little decrease from 5 cm to the top in the K-concentration, followed by a decrease to the bed rock

(Appendix II 4), profile 9 shows a totally different trend compared to profile 2. Profile 8 however also starts with a decrease towards the surface, but stabilizes towards parent rock. The Fe-concentration (Appendix II 2) is the highest in a depth of 10 cm at profile 9. Since this site does not behave similar to profile 2 and 8, it could be possible, that profile 9 is affected by tsunamis the most. This assumption is based on the high Fe-concentration at 10 cm. Since the precipitation is little, dislocations of the elements are not likely to happen as clearly as it is shown in profile 9. Therefore, the accumulation of Fe, Mn and Ti (Appendix II 2, 5 and 6,) is assumed been induced by tsunamis.

6.1.4. Delta

The focus at this site will be profile 3. Profile 3* is also in the dead zone, but only the uppermost and the lowest part of the profile have been analysed, which makes this profile little predicating. All soils at this site, except for profile 15, are very sandy soils, whereas profile 15 is rather mire-like. The first 15 cm of profile 3 do not contain a lot of organic material. The highest amount of the organic content could be measured in a depth of 20 cm. Profile 13 acts similar to profile 3 concerning the LOI. Profile 13 is located in the affected zone and therefore shows a resembling trend. Similar to profile 9, the organic material starts to increase towards the bed rock. This lack of organic material in the upper 15 cm of site 3 can also be observed in the Si-concentration (Fig. 24). This concentration reaches its minimum at 20 cm. At this depth, the most organic material was measured. Since Al (Appendix II 1) reach its minimum concentration at 20 cm, it can be assumed that an eluviation and a displacement, caused by tsunamis, occurred. The lowest Fe-concentration (Appendix II 2) was measured at 25 cm. The Na-concentration (Fig. 23) starts to decrease at 15 cm. A possible reason for the high Na-concentration between 0 cm and 15 cm is the soil structure. The organic layer, which starts at 15 cm, could retain Na of a displacement in bigger depths.

6.1.5. pH

The value of the pH is influenced by the vegetation, but also by the material of the bed rock. Granites and orthogenesis dominate in this area as parent rock material (Weidick et al., 2007). Due to the missing carbonates in these crystalline rock, they are not able to buffer the ph. This leads to acidic conditions in the soils (Scheffer et al., 2002).

The pH of profile 2, 3, 8 and 9 in Figure 27 show similar characteristics. They are all increasingly acidic, sometimes rapidly (profile 3, 8 and 9), towards the bed rock. But also, other profiles like 6, 13 and 14 act in a similar way, even though they are not in the dead zone as opposed to the other profiles. Profile 13 is in the affected zone and profile 6 and 14 are in the transition zone. Big tsunami waves might have reached their location and therefore increased their pH in the upper soil as McLeod et al. (2010) explain.

6.1.6. C/N

The C/N ratio is a ratio for nutrients and indicates how easily the microbes can decompose organic material in soil (Wang et al., 2014). It is expected, that higher C/N ratios are measured on the top of the profile with a continuous decrease towards parent rock. All profiles show more or less unobtrusive trends, except for the profiles at Camp Site. Due to the cryoturbation and other disturbances in the soil, the C/N ratios were expected to show not typical trends. As an example, the C/N ratio decreases with increasing depth in alpine soils, because the microbes use C and N sticks to the clay minerals and therefore cannot be decomposed easily.

6.1.8. Improvements

For a better geochemical resolution, the profiles should have been sampled equally, e.g. every 5 cm. This was not the case in some of the profiles. In particular, profile 3*, 5, 7, 12 and 15, only the uppermost and the lowest horizon have been sampled. But the most interesting profiles for this thesis are those sites in the dead zone. It might have been useful, if more samples were taken in the dead zone to gain better statistics. Furthermore, more caution is needed during sampling to avoid mistakes such as at site 3, where an inverse age resulted.

6.2. Radiocarbon-dating

The radiocarbon age from profile 3 at Delta indicates an age inversion. Normally the oldest sample should be found at the bottom of the soil, as was done in profile 5, 6, 7 and 13, shown in table 1. An explanation of this inversed age as in profile 3 could be, that the bottom has been contaminated by recent organic material like roots which belongs to an upper part of the soil. This could have happened during digging out the profile.

Further, the more a material is weathered, the older it is. Therefore, the weathering ratio should decrease with increasing age and should correlate with the radiocarbon-dating. But a correlation with the weathering index (Ca+K)/Ti (Fig. 25) and the ^{14}C ages (Table 1) does not seem possible with old samples. For example, profile 5 has an age of 9550–9494 cal. BP (2σ) in a depth of 63 cm. Hence, the weathering index would be expected to be low. But with a ratio of 19 this soil sample is less weathered. Further, profile 13 with an age of 8329–8176 cal. BP (2σ) at 23 cm has a ratio of 21. However, younger samples seem to correlate better. Profile 7 has a modern age and is not weathered well.

An explanation for the correlation between the weathering index and the ^{14}C does not work as expected could be the particle size. While physical weathering increases the surface by decreasing the grain size, the vulnerability to chemical weathering increases (Blume et al., 2009). The material at Delta is very sandy and the particle size is bigger compared to the material at the other sites. Hence, the particles at site Delta are assumed to be exposed less to chemical weathering which would explain the high weathering ratio.

All the samples which were pretreated with the AAA-technique present young ages (oldest: 910–743 cal. BP). Therefore, it can be assumed that a lot of disturbances occurred around 910–743 cal. BP already. Additionally, the problem of cryoturbation is present, which is a dominant pedologic process in permafrost areas. Favorable conditions for cryoturbation is permafrost within the first 1 m, freeze-thaw cycles, conditions of poor drainage and a parent material enriched with silt (Bockheim and Tarnocai, 1998). Due to the cryoturbation, younger material can be transported downwards and older upwards which affects the ^{14}C results.

The ages from profile 5 and 13 suit the ages from literature very well. The minimum age of deglaciation at the eastern Disko Bugt was dated back to 10.3 ka BP. The Eqip Sermia is located more in the eastly and therefore its deglaciation started later (Weidick et al., 2007). A moraine system along West Greenland was investigated. The system passes by Eqip Sermia, where a shell from the southern flank of the glacier was dated. The shell has an age of 7.3 ka BP (Weidick et al., 2007). This age is very close to the calibrated radiocarbon ages in this work. Since the shell was collected near the glacier and the examined samples are further away from the glacier, it makes sense that the samples are older than the dated shell.

Zooming out and considering deglaciations in other regions of the world allows to put this finding into context. Depending on the geographic location the Last Glacial Maximum ended between approximately 19 ka and 11 ka (Clark et al., 2012). Going from North to South, the

Fennoscandia got deglaciated after 12.5 ka (Nygård et al., 2004), whereas Latvia became ice-free between 14 ka–12 ka BP (Ehlers & Gibbard, 2004). The deglaciation in northern America could be dated with moraines in the Lake Superior region that have an age of 11 ka (Saarnisto, 1974). The alpine deglaciation started 14 ka ago (Ravazzi, 2002). The higher the latitude, the later the deglaciation should be, but climatic conditions influence the start of the deglaciation.

6.3. Cross-dating

During the working process, a few uncertainties occurred. Per plant, species and site, only one reference plant has been sampled in a zone, where the plants were obviously not affected by tsunamis. These reference plants cannot be verified, because for a reference chronology of the site, at least 10-15 plant would have to be analyzed. Furthermore, there were also no other data available, neither in literature nor in other data bases (e.g. from the shrub hub). Thus, the assignment of calendar years to the rings is not absolute, as no other reference plants near the study site are present. Furthermore, the three sites vary in microclimatic conditions and therefore a suitable reference plant is difficult to find. It is known that microsite conditions highly influence the annual growth (Young etl a., 2016). Nevertheless, the 6 (three main sites with one BN and one SA) reference plants were convenient for a relative cross-dating.

Another uncertainty is the plant 13B in figure 31 as already described in the result section (chapter 5.2.1.). The variation of the annual rings from 13B could also be due to local changes in the site factors like temperature, precipitation or probable changes in groundwater surface in mire areas which affects the growth of the vegetation. The site, where this SA was collected, was very dry and sandy. Besides no BN could be found. The conditions might be better for the SA than for the BN, whereby the BN grows as well on bogs as on rocky and sandy soils with acidic (pH 4-5) conditions (Groot et al., 1997). Even though this site is visibly affected by tsunamis, due to accumulations of sand, rock and shells, the SA seemed to grow well. It is possible, that the height and the frequency of the tsunamis reached their maximum in 2008 and 2012 and decreased after 2012 which allowed the plant to recover.

It can be assumed, that in the years (1971, 1973, 1978, 1985, 1990, 1993 and 1996) big tsunami-events happened. It is possible that in 1985 and 1993 even bigger tsunamis occurred, due to the reduction of the annual ring growth in the plants 10B and 14A (1985) and 7A and 10B (1993). These plants were the closest to the shore compared to the other dwarf shrubs in the transition

zone (Fig. 32). Another reason for a decrease of the ring width through these years could also be due to climatic variations. A comparison with climatic data has not been made, because the changes in ring widths do not show the same trend in the dead and transition zone in the mentioned years, except in 1985 and 1993. However, to exclude possible tsunami-events in 1985 and 1993 temperature and precipitation measurements should have been considered as well. Nevertheless, the research questions could be answered without any consideration of climatic data.

Even though, long term chronologies in dendrogeomorphic researches are unusual, due to the limited information of annual ring width measurement (Shroder, 1980), useful information about tsunami-events could be gathered. The hypothesis from Lüthi et al. (2016), that large tsunami-waves of 15–20 m and the active erosion of soil and vegetation up to 20 m a.s.l. started in 2012, can be rejected with the results from the dendrochronology. Additionally, Nielsen (1992) mentions a report from 1962/64, that ponds of sea water with living benthic marine animals at an elevation of 12–15m a.s.l. were found. This rejects the hypothesis that no large tsunamis occurred before 2012.

6.2.1. Improvements

Even though this research is not very representative due to the small sample size, it shows that the dwarf shrubs in the dead zone react with a decrease in the annual ring growth when tsunamis assumedly have occurred. But to improve the accuracy and provide an absolute chronology, a transect would be helpful and 10 to 15 plants should be sampled at each site. Furthermore, missing rings had to be inserted during the cross-dating, which can distort the results. For these discontinuous or missing rings, approximately 20 radii should be measured per cross-section which allows the missing or discontinues rings to be detected better.

7. Conclusion

Successfully more information about the area at the Eqip Sermia were gained. Data from literature could be verified and hypothesis from other authors could be rejected with the results from this Master's Thesis. Soil samples from the mire-like and sandy soils and samples from BN and SA located at the landscape facing the calving front were used. Geochemical and dendrochronological investigations and radiocarbon-dating were conducted to gain data about soil properties, tsunami-history and deglaciation. Therefore, the start of the soil formation and the occurrences of tsunamis caused by calving-events from the Eqip Sermia could be investigated.

In the beginning, these three research questions were formulated:

- *"How suitable is the geochemical analysis of mire like and sandy soils, radiocarbon-dating and the dendrochronological analysis of the dwarf shrubs BN and SA to deduce tsunami-events?"*
- *"Have other large tsunami-events occurred before 2012, caused by calving from the Eqip Sermia?"*
- *"Is it possible to measure the quantity of the tsunami-events?"*

The geochemical analysis has shown expected and typical trends in LOI, XRF and pH for most of the profiles next to the shore, whereas the elevation of the profile affected the results in this analysis. With the radiocarbon-dating the beginning of the soil formation could be dated back to 9546–9523 cal. BP. Further, the samples with an AAA-pre-treatment showed recent ages. This indicates disturbances during soil formation; in this case rather cryoturbation than tsunamis. Age correlations with XRF and ^{14}C were not possible. Therefore, the geochemical analysis presents only qualitative results. The dendrochronology can only be used for investigating recent events, due to the lifespan of the plants. Nevertheless, decreases in annual ring widths were measured, which are assumingly caused by tsunamis. With those methods, it is possible to deduce tsunami-events. However, only qualitative data with geochemistry and relative ages with dendrochronology were gained.

Since geochemistry presents qualitative results, it is not possible to answer the second research question with this analysis. Based on the dendrochronological analysis it can be assumed that large tsunami-events occurred before 2012. The results also show that years with tsunami occurrences can be dated. Albeit, the analysis does not show how many tsunamis were triggered

within a year. Therefore, dendrochronology shows a low temporal resolution using the analysis of the ring width.

Even though, there is no absolute chronology concerning tsunami-events, a relative chronology could be reconstructed. It would be worth to do further and more detailed investigations in this topic. Finally, despite of the low number of samples, useful results have been achieved. Nevertheless, the results should be treated with consideration.

8. References

Amundson, J. M., & Truffer, M. (2010). A unifying framework for iceberg-calving models. *Journal of Glaciology*, *56*(199), 822–830. https://doi.org/10.3189/002214310794457173

Amundson, J. M., Truffer, M., Lüthi, M. P., Fahnestock, M., West, M., & Motyka, R. J. (2008). Glacier, fjord, and seismic response to recent large calving events, Jakobshavn Isbræ, Greenland. *Geophysical Research Letters*, *35*(22), 1–5. https://doi.org/10.1029/2008GL035281

Becker, B. (1992). The History of Dendrochronology and Radiocarbon Calibration. In *Radiocarbon After Four Decades* (pp. 34–49). New York, NY: Springer New York. https://doi.org/10.1007/978-1-4757-4249-7_4

Blaauw, M., & Christen, J. A. (2005). Radiocarbon peat chronologies and environmental change. *Journal of the Royal Statistical Society. Series C: Applied Statistics*, *54*(4), 805–816. https://doi.org/10.1111/j.1467-9876.2005.00516.x

Blok, D., Sass-Klaassen, U., Schaepman-Strub, G., D. Heijmans, M. M. P., Sauren, P., & Berendse, F. (2011). What are the main climate drivers for shrub growth in Northeastern Siberian tundra? *Biogeosciences*, *8*(5), 1169–1179. https://doi.org/10.5194/bg-8-1169-2011

Blume, H., Brümmer, G., & Horn, R. (2009). *Scheffer/Schachtschabel: Lehrbuch der Bodenkunde*. Retrieved from https://books.google.ch/books?hl=de&lr=&id=6SkpBAAAQBAJ&oi=fnd&pg=PR5&dq=SCHEFFER,+F.+%26+Schachtschabel,+P.+(2010).+Lehrbuch+der+Bodenkunde.+16.+Auflage.+Spektrum+Akademischer+Verlag.&ots=EAmb9pPI0w&sig=h_6GwBrINMc_n6ewnGhSiFYYBNY

Bockheim, J. G., & Tarnocai, C. (1998). Recognition of cryoturbation for classifying permafrost-affected soils. *Geoderma*, *81*(3–4), 281–293. https://doi.org/10.1016/S0016-7061(97)00115-8

Boxleitner, M., Musso, A., Waroszewski, J., Malkiewicz, M., Maisch, M., Dahms, D., … Egli, M. (2017). Late Pleistocene – Holocene surface processes and landscape evolution in the central Swiss Alps. *Geomorphology*, *295*, 306–322. https://doi.org/10.1016/j.geomorph.2017.07.006

Bradley, R. S., Vuille, M., Diaz, H. F., & Vergara, W. (2006). Climate change. Threats to water supplies in the tropical Andes. *Science (New York, N.Y.)*, *312*(5781), 1755–6. https://doi.org/10.1126/science.1128087

Bronk Ramsey, C. (2001). Development of the radiocarbon calibration program. *Radiocarbon*, *43*(2), 355–363. https://doi.org/papers2://publication/uuid/5B399323-3576-4144-BF98-497069142583

Bronk Ramsey, C. (2009). Bayesian Analysis of Radiocarbon Dates. *Radiocarbon*, *51*(1), 337–360. https://doi.org/10.2458/azu_js_rc.v51i1.3494

Camarero, J. J., Guerrero-Campo, J., & Gutiérrez, E. (1998). Tree-Ring Growth and Structure of Pinus uncinata and Pinus sylvestris in the Central Spanish Pyrenees. *Arctic and Alpine Research*, *30*(1), 1–10. https://doi.org/10.2307/1551739

Chambers, F. M., & Charman, D. J. (2004). Holocene environmental change: contributions from the peatland archive. *The Holocene*, *14*(1), 1–6. https://doi.org/10.1191/0959683604hl684ed

Clark, P. U., Shakun, J. D., Baker, P. A., Bartlein, P. J., Brewer, S., Brook, E. J., … Williams, J. W. (2012). Global climate evolution during the last deglaciation. *Proceedings of the National Academy of Sciences of the United States of America*, *109*(19), 1134–1142. https://doi.org/10.1073/pnas.1116619109/-/DCSupplemental.www.pnas.org/cgi/doi/10.1073/pnas.1116619109

Desloges, J. R., Gilbert, R., Nielsen, N., Christiansen, C., Rasch, M., & Øhlenschläger, R. (2002). Holocene glacimarine sedimentary environments in fiords of Disko Bugt, West Greenland. *Quaternary Science Reviews*, *21*(8–9), 947–963. https://doi.org/10.1016/S0277-3791(01)00049-X

Egli, M., Brandová, D., Röthlisberger, S., Woodhatch, I., & Zollinger, B. (2016). *Geochronology Laboratory Methods*.

Egli, M., Nater, M., Mirabella, A., Raimondi, S., Plötze, M., & Alioth, L. (2008). Clay minerals, oxyhydroxide formation, element leaching and humus development in volcanic soils. *Geoderma*, *143*(1–2), 101–114. https://doi.org/10.1016/j.geoderma.2007.10.020

Ehlers, J., & Gibbard, P. L. (2004). *Quaternary Glaciations Extent and Chronology - Part I: Europe*. *Developments in Quaternary Sciences* (Vol. 2). Elsevier.

https://doi.org/10.1016/S1571-0866(04)80056-3

Fumal, T., & Seitz, G. (1999). *Implications of paleoseismicity for rupture behavior of south-central San Andreas Fault*. *The Paleoseismology Workshop*. Retrieved from https://pdfs.semanticscholar.org/544e/168d58f5f7ce093f63165a771f174b54ef71.pdf#page=39

Gärtner, H., & Schweingruber, F. H. (2013). *Microscopic Preparation Techniques for Plant Stem Analysis*. Verlag Dr. Kessel, Remagen.

Gierlowski-Kordesch, E. (2004). Paleolimnology: The History and Evolution of Lake Systems. *PALAIOS*, *19*(2), 184–186. https://doi.org/10.1669/0883-1351(2004)019<0184:BR>2.0.CO;2

Groot, W. J., Thomas, P. A., & Wein, R. W. (1997). Betula Nana L. and Betula Glandulosa Michx. *Journal of Ecology*, *85*(2), 241–264. https://doi.org/10.2307/2960655

Halpern, D. (2016). *Master Thesis Investigation of Volcanic Sediments on the Nebrodi Mountains*.

Hansen, B. U., Elberling, B., Humlum, O., & Nielsen, N. (2006). Meteorological trends (1991–2004) at Arctic Station, Central West Greenland (69°15'N) in a 130 years perspective. *Geografisk Tidsskrift-Danish Journal of Geography*, *106*(1), 45–55. https://doi.org/10.1080/00167223.2006.10649544

Hollesen, J., Buchwal, A., Rachlewicz, G., Hansen, B. U., Hansen, M. O., Stecher, O., & Elberling, B. (2015). Winter warming as an important co-driver for Betula nana growth in western Greenland during the past century. *Global Change Biology*, *21*(6), 2410–2423. https://doi.org/10.1111/gcb.12913

Howat, I. M., Joughin, I., Fahnestock, M., Smith, B. E., & Scambos, T. A. (2008). Synchronous retreat and acceleration of southeast Greenland outlet glaciers 2000-06: Ice dynamics and coupling to climate. *Journal of Glaciology*, *54*(187), 646–660. https://doi.org/10.3189/002214308786570908

IPCC. (2014). *Contribution of Working Groups I, II and III to the Fifth Assessment Report of the Intergovernmental Panel on Climate Change*. *Climate Change 2014: Synthesis Report*. https://doi.org/10.1017/CBO9781107415324

J. A. P. Paiva J. C. Rodrigues, A. Alves, S. Santos, J. Graça, G. Le Provost, P. Chaumeil, D. Da Silva-Perez, A. Bosc, P. Fevereiro, C. Plomion, P. H. G.-G. (2008). Plasticity of maritime pine (Pinus pinaster) wood-forming tissues during a growing season. *New Phytologist*, *179*, 1180–1194. https://doi.org/10.1111/j.1469-8137.2008.02536.x

Jäger, H. (2013). *Moorsedimente als Spiegelbild von Erosion und Bodenbildung*.

Jia, G. J., Epstein, H. E., & Walker, D. A. (2009). Vegetation greening in the canadian arctic related to decadal warming. *Journal of Environmental Monitoring*, *11*(12), 2231–2238. https://doi.org/10.1039/b911677j

Jr, J. S. (1980). Dendrogeomorphology: review and new techniques of tree-ring dating. *Progress in Physical Geography*, 161–188. Retrieved from http://journals.sagepub.com/doi/abs/10.1177/030913338000400202

Juan, J. De, Elósegui, P., Nettles, M., Larsen, T. B., Davis, J. L., Hamilton, G. S., … Forsberg, R. (2010). Sudden increase in tidal response linked to calving and acceleration at a large Greenland outlet glacier. *Geophysical Research Letters*, *37*(12), 1–5. https://doi.org/10.1029/2010GL043289

Kappas, M. (2009). *Klimatologie: Klimaforschung im 21. Jahrhundert-Herausforderung für Natur-und Sozialwissenschaften*. Retrieved from https://books.google.ch/books?hl=de&lr=&id=8yogBAAAQBAJ&oi=fnd&pg=PR3&dq=Klimatologie.+Klimaforschung+im+21.+Jahrhundert-+Herausforderung+für+Natur-+und+Sozialwissenschaften.&ots=cjoMLbc5fA&sig=O3XmIvPdeOeHjRQVetOEHf8xAl8

Kniveton, D. (2007). Encyclopedia of World Climatology - Edited by John E Oliver. *Geographical Journal*, *173*(1), 93–94. https://doi.org/10.1111/j.1475-4959.2007.233_2.x

Kretschmann, D., & Cramer, S. (2007). The role of earlywood and latewood properties on dimensional stability of loblolly pine. *Proceedings of the Compromised Wood Workshop*, *January 29*(Larson 1969), 1–24. Retrieved from http://128.104.77.228/documnts/pdf2007/fpl_2007_kretschmann002.pdf

Kylander, M. E., Bindler, R., Cortizas, A. M., Gallagher, K., Mörth, C. M., & Rauch, S. (2013). A novel geochemical approach to paleorecords of dust deposition and effective humidity: 8500 years of peat accumulation at Store Mosse (the "Great Bog"), Sweden.

Quaternary Science Reviews, *69*, 69–82. https://doi.org/10.1016/j.quascirev.2013.02.010

Li, X., Wu, H. X., & Southerton, S. G. (2010). Seasonal reorganization of the xylem transcriptome at different tree ages reveals novel insights into wood formation in Pinus radiata. *New Phytologist*, *187*(3), 764–776. https://doi.org/10.1111/j.1469-8137.2010.03333.x

Logsdon, S. (2008). Encyclopedia of Soil Science. *Soil Science Society of America Journal*, *72*, 862. https://doi.org/10.2136/sssaj2008.0003br

Lüthi, M. P., & Vieli, A. (2016). Multi-method observation and analysis of a tsunami caused by glacier calving. *Cryosphere*, *10*(3), 995–1002. https://doi.org/10.5194/tc-10-995-2016

Lüthi, M. P., Vieli, A., Moreau, L., Joughin, I., Reisser, M., Small, D., & Stober, M. (2016). A century of geometry and velocity evolution at Eqip Sermia, West Greenland. *Journal of Glaciology*, 1–15. https://doi.org/10.1017/jog.2016.38

Maas, H., Schwalbe, E., Dietrich, R., Bässler, M., & Ewert, H. (2007). Determination of spatio-temporal Velocity Fields on Glaciers in West-Greenland by Terrestrial Image Sequence Analysis. *International Archives of Photogrammetry and Remote Sensing*, *2003*, 2004–2009. Retrieved from https://tu-dresden.de/die_tu_dresden/fakultaeten/fakultaet_forst_geo_und_hydrowissenschaften/fachrichtung_geowissenschaften/ipf/photogrammetrie/publikationen/pubdocs/2008/2008_Maas_ISPRS2008.pdf

McLeod, M. K., Slavich, P. G., Irhas, Y., Moore, N., Rachman, A., Ali, N., … Caniago, C. (2010). Soil salinity in Aceh after the December 2004 Indian Ocean tsunami. *Agricultural Water Management*, *97*(5), 605–613. https://doi.org/10.1016/j.agwat.2009.10.014

Moon, T., & Joughin, I. (2008). Changes in ice front position on Greenland's outlet glaciers from 1992 to 2007. *Journal of Geophysical Research: Earth Surface*, *113*(2), 1–10. https://doi.org/10.1029/2007JF000927

Musso, A. (2016). *Reconstruction of Holocene landscape evolution using mires situated in the Göschenen valley*.

Myers-Smith, I., & Elmendorf, S. (2015a). Climate sensitivity of shrub growth across the tundra biome. *Nature Climate Change*, *5*, 887–892. https://doi.org/10.1038/nclimate2697

Myers-Smith, I. H., Hallinger, M., Blok, D., Sass-Klaassen, U., Rayback, S. A., Weijers, S., … Wilmking, M. (2015b). Methods for measuring arctic and alpine shrub growth: A review. *Earth-Science Reviews*. https://doi.org/10.1016/j.earscirev.2014.10.004

Nielsen, N. (1992). A boulder beach formed by waves from a calving glacier; Eqip Sermia, West Greenland. *Boreas*, *21*(2), 159–168. https://doi.org/10.1111/j.1502-3885.1992.tb00023.x

Nygård, A., Sejrup, H. P., Haflidason, H., Cecchi, M., & Ottesen, D. (2004). Deglaciation history of the southwestern Fennoscandian Ice Sheet between 15 and 13 14C ka BP. *Boreas*, *33*(1), 1–17. https://doi.org/10.1111/j.1502-3885.2004.tb00992.x

Piotrowska, N., Blaauw, M., Mauquoy, D., & Chambers, F. M. (2011). Constructing deposition chronologies for peat deposits using radiocarbon dating. *Mires and Peat*, *7*(10), 1–14. https://doi.org/10.1111/j.1365-2486.2009.01920.x

Post, A., O'Neel, S., Motyka, R. J., & Streveler, G. (2011). A complex relationship between calving glaciers and climate. *Eos*, *92*(37), 305–307. https://doi.org/10.1029/2011EO370001

Ravazzi, C. (2002). Late Quaternary history of spruce in southern Europe. *Review of Palaeobotany and Palynology*, *120*(1–2), 131–177. https://doi.org/10.1016/S0034-6667(01)00149-X

Reimer, P. J., Bard, E., Bayliss, A., Beck, J. W., Blackwell, P. G., Ramsey, C. B., … van der Plicht, J. (2013). IntCal13 and Marine13 Radiocarbon Age Calibration Curves 0–50,000 Years cal BP. *Radiocarbon*, *55*(4), 1869–1887. https://doi.org/10.2458/azu_js_rc.55.16947

Rignot, E., Koppes, M., & Velicogna, I. (2010). Rapid submarine melting of the calving faces of West Greenland glaciers. *Nature Geoscience*, *3*(3), 187–191. https://doi.org/10.1038/ngeo765

Saarnisto, M. (1974). The deglaciation history of the Lake Superior region and its climatic implications. *Quaternary Research*, *4*(3), 316–339. https://doi.org/10.1016/0033-5894(74)90019-2

Scambos, T. A., Hulbe, C., Fahnestock, M., & Bohlander, J. (2000). The link between climate warming and break-up of ice shelves in the Antarctic Peninsula. *Journal of Glaciology*,

46(154), 516–530. https://doi.org/10.3189/172756500781833043

Scheffer, F., Schachtschabel, P., Blume, H., Brummer, G. W., Schwertmann, U., Hörn, R., … Wilke, B. (2002). *Lehrbuch der Bodenkunde*.

Schweingruber, F., & Büntgen, U. (2013). What is "wood"–An anatomical re-definition. *Dendrochronologia*, *31*, 187–191. Retrieved from http://www.sciencedirect.com/science/article/pii/S1125786513000441

Schweingruber, F. H. (1988). *Tree Rings: Basics and Applications of Dendrochronology*. *Kluwer Academic Publishers*. https://doi.org/10.1007/978-94-009-1273-1

Schweingruber, F. H. (1996). *Tree rings and environment. Dendroecology. Landscape*. https://doi.org/10.2307/1224418

Schweingruber, F. H., Braun, S., Nievergelt, D., Hellmann, L., Tegel, W., & Büntgen, U. (2013). Evaluating the wood anatomical and dendroecological potential of arctic dwarf shrub communities. *IAWA Journal*, *34*(4), 485–497. https://doi.org/10.1163/22941932-00000039

Schweingruber, F., & Poschlod, P. (2005). Growth rings in herbs and shrubs: life span, age determination and stem anatomy. *Forest Snow and Landscape Research*, *79*(3), 195–415. Retrieved from http://www.wsl.ch/dienstleistungen/publikationen/pdf/79_3_7276.pdf

Serreze, M. C., & Francis, J. a. (2006). The Arctic on the fast track of change. *Weather*, *61*, 65–69. https://doi.org/10.1256/wea.197.05

Veit, H. (2002). *Die Alpen: Geoökologie und Landschaftsentwicklung*. Retrieved from https://scholar.google.ch/scholar?hl=de&q=Die+Alpen+–+Geoökologie+und+Landschaftsentwicklung.+Verlag+Eugen+Ulmer.+Stuttgart.&btnG=&lr=

Walker, D. A., Raynolds, M. K., Daniëls, F. J. A., Einarsson, Elvebakk, ;, Arve, … Katenin, A. E. (2005). The Circumpolar Arctic vegetation map. *Journal of Vegetation Science*, *16*, 267–282. https://doi.org/10.1111/j.1654-1103.2005.tb02365.x

Wang, M., Moore, T. R., Talbot, J., & Richard, P. J. H. (2014). The cascade of C:N:P stoichiometry in an ombrotrophic peatland: from plants to peat. *Environmental Research*

Letters, *9*(2), 1–7. https://doi.org/10.1088/1748-9326/9/2/024003

Warren, C. R. (1993). Rapid Recent Fluctuations of the Calving San-Rafael Glacier, Chilean Patagonia - Climatic or Non-Climatic. *Geografiska Annaler Series A-Physical Geography*, *75*(3), 111–125. https://doi.org/10.2307/521029

Weidick, A., Bennike, O., & Grafisk, S. (2007). *Quaternary glaciation history and glaciology of Jakobshavn Isbrae and the Disko Bugt region, West Greenland: a review*. *Geological Survey of Denmark and Greenland Bulletin* (Vol. 14). Retrieved from https://www.researchgate.net/profile/Ole_Bennike/publication/282736999_Quaternary_glaciation_history_and_glaciology_of_Jakobshavn_Isbrae_and_the_Disko_Bugt_region_West_Greenland_A_review/links/5685211108ae051f9af1a70c.pdf

Weijers, S., Wagner-Cremer, F., Sass-Klaassen, U., Broekman, R., & Rozema, J. (2013). Reconstructing High Arctic growing season intensity from shoot length growth of a dwarf shrub. *The Holocene*, *23*(5), 721–731. https://doi.org/10.1177/0959683612470178

Wimmer, R. (2002). Wood anatomical features in tree-rings as indicators of environmental change. *Dendrochronologia*, *20*(1), 21–36. https://doi.org/10.1078/1125-7865-00005

Young, A. B., Watts, D. A., Taylor, A. H., & Post, E. (2016). Species and site differences influence climate-shrub growth responses in West Greenland. *Dendrochronologia*, *37*, 69–78. https://doi.org/10.1016/j.dendro.2015.12.007

9. Appendix

Appendix I: Geochemistry

		Depth [cm]	XRF-LOI [%]	Na	Mg	Al	Si	P	K	Ca	Ti	Mn	Fe	Rb	Zr	LOI Average [%]	Anorganic [%]	C/N	pH
Camp Site	Profile 1	0	58	1,926	1,045	3,782	19,117	0,139	1,173	1,968	0,201	0,0516	1,6933	0,00500	0,01791	18,1993	81,801	18	5,35
		2,5	59	2,06	0,899	3,89	19,721	0,128	1,218	1,946	0,205	0,0511	1,7124	0,00499	0,01752	18,0668	81,933	18,44	5,35
		5	60	2,191	0,62	4,34	23,858	0,099	1,479	1,999	0,146	0,022	1,2377	0,00532	0,02202	12,1565	87,844	20,27	5,2
		7,5	61	2,329	0,602	4,666	26,025	0,091	1,565	2,082	0,151	0,0214	1,2148	0,00552	0,02289	9,00185	90,998	20,85	5,3
		10	62	2,055	0,531	4,469	24,511	0,081	1,5	2,09	0,16	0,0226	1,2511	0,00553	0,02339	11,895	88,105	24,2	5,4
	Profile 2	0	37	1,882	0,614	3,692	19,4	0,107	1,115	1,822	0,13	0,0343	1,2719	0,00421	0,01769	18,314	81,686	16,39	5,15
		3	38	1,596	0,466	3,193	15,898	0,088	0,935	1,665	0,106	0,0297	1,2212	0,00324	0,01253	27,9973	72,003	16,54	5,1
		6	39	1,978	0,473	3,921	21,536	0,094	1,246	1,665	0,121	0,0129	1,0899	0,00402	0,01479	17,866	82,134	15,06	5,05
		9	40	2,509	0,576	5,2	29,171	0,094	1,755	1,794	0,165	0,0156	1,0884	0,00585	0,02765	5,68599	94,314	13,33	4,9
	Profile 4	0	63	2,756	1,035	5,426	22,397	0,134	1,673	1,519	0,298	0,0461	2,1048	0,00470	0,01753	11,2658	88,734	20,23	5,4
		5	64	3,089	1,099	5,974	25,238	0,128	1,887	1,535	0,299	0,0435	2,0366	0,00503	0,01826	6,49045	93,51	21,45	5,45
		10	65	2,823	0,971	5,536	23,062	0,146	1,681	1,622	0,266	0,0439	2,0122	0,00486	0,0174	9,80683	90,193	19,3	5,5
		15	66	2,282	0,525	4,927	26,753	0,084	1,651	1,944	0,166	0,0271	1,3166	0,00582	0,02547	8,44442	91,556	22,04	5,5

		Depth [cm]	XRF-LOI [%]	Na	Mg	Al	Si	P	K	Ca	Ti	Mn	Fe	Rb	Zr	LOI Average [%]	Anorganic [%]	C/N	pH
Fox Beach	Profile 5	0-5	145	2,297	0,739	5,497	28,256	0,064	1,592	1,844	0,191	0,0395	1,7327	0,00569	0,01892	8,08219	91,918	18,11	4,95
		61-66	146	2,043	0,808	5,667	25,572	0,187	1,448	1,659	0,161	0,034	1,5888	0,00573	0,00765	7,68295	92,317	16,59	4,75
	Profile 6	0	147	1,986	0,778	5,011	24,376	0,098	1,434	1,78	0,177	0,0334	1,6414	0,00542	0,01226	11,0364	88,964	19	5,3
		5	148	2,472	0,671	5,567	31,942	0,017	1,643	1,761	0,136	0,0224	1,2895	0,00577	0,00844	1,26103	98,739	16,06	5,2
		10	149	2,534	0,748	5,86	30,969	0,038	1,79	1,861	0,168	0,0225	1,5582	0,00638	0,00937	2,43038	97,57	18	4,9
		15-20	150	2,127	0,733	5,396	26,82	0,091	1,564	1,714	0,173	0,0198	1,2541	0,00591	0,00988	7,51605	92,484	17,79	4,7
		22-27	151	1,998	0,759	5,161	25,37	0,092	1,476	1,618	0,183	0,0183	1,0713	0,00536	0,0133	12,3354	87,665	17,01	4,65
	Profile 7	0-5	152	1,604	0,666	2,825	14,677	0,044	0,892	1,168	0,11	0,0129	1,0254	0,00316	0,00885	30,0079	69,992	28,82	5,2
		9-14	153	1,954	0,717	4,278	19,504	0,105	1,222	1,369	0,128	0,0321	1,4467	0,00478	0,01107	17,2847	82,715	18,42	5,3
	Profile 8	0	155	2,655	0,904	5,325	27,663	0,057	1,54	1,522	0,151	0,0241	1,3562	0,00560	0,00843	5,49174	94,508	16,94	5,2
		5	156	2,396	0,955	5,603	26,691	0,068	1,667	1,491	0,147	0,0286	1,4554	0,00609	0,00755	7,41812	92,582	7,489	5,1
		10	157	2,406	0,928	5,467	27,75	0,067	1,671	1,59	0,169	0,023	1,4801	0,00607	0,01243	5,54689	94,453	12,97	4,8

Appendix I 1: *Geochemistry, Site Camp Site and Fox Beach.*

		Depth [cm]	XRF-LOI [%]	Na	Mg	Al	Si	P	K	Ca	Ti	Mn	Fe	Rb	Zr	LOI Average [%]	Anorganic [%]	C/N	pH
Charlie	Profile 9	0	158	2,478	0,932	4,344	23,641	0,07	1,291	1,685	0,218	0,0202	1,5243	0,00473	0,0189	12,7961	87,204	19,21	5,3
		5	159	2,615	1,538	5,075	29,621	0,086	1,49	1,812	0,371	0,0399	2,4805	0,00552	0,01815	2,72356	97,276	13,47	5,3
		10	200	2,56	1,75	5,156	26,201	0,125	1,378	1,746	0,402	0,057	2,8158	0,00551	0,01907	5,95347	94,047	13,85	5,4
		15-20	201	1,777	0,881	3,907	17,549	0,142	1,075	1,516	0,228	0,0282	2,0924	0,00450	0,0156	20,9502	79,05	15,64	4,8
	Profile 10	0	202	2,198	0,903	5,177	28,837	0,065	1,485	2,011	0,233	0,0319	1,738	0,00555	0,01922	4,45046	95,55	15,5	5,3
		5	203	2,1	0,948	5,009	27,385	0,077	1,502	1,965	0,196	0,0285	1,6441	0,00582	0,01485	4,58148	95,419	14,45	5,4
		10	204	2,265	0,97	5,398	29,744	0,059	1,567	1,92	0,193	0,0266	1,6332	0,00584	0,012	2,95741	97,043	13,07	5,4
		15	205	2,359	0,837	5,118	29,754	0,063	1,487	1,968	0,196	0,0243	1,4794	0,00557	0,01307	2,92345	97,077	16	5,4
		20	206	2,48	0,897	5,483	30,591	0,044	1,589	1,935	0,189	0,0258	1,5815	0,00563	0,01198	2,85639	97,144	11,9	5,4
		25	207	2,047	0,94	4,84	25,184	0,11	1,404	1,926	0,205	0,0227	1,6768	0,00555	0,01328	7,8179	92,182	16,35	5,3
		30	208	2,285	0,979	5,039	26,998	0,084	1,451	2,013	0,233	0,0228	1,7407	0,00556	0,01645	6,05957	93,94	15,5	5,2
		35	209	1,959	0,745	4,331	21,844	0,101	1,254	1,855	0,185	0,0205	1,8725	0,00488	0,01537	13,8299	86,17	17,14	5,2
		40	210	1,943	0,796	4,592	23,832	0,101	1,344	1,911	0,213	0,0226	1,9293	0,00517	0,02358	11,3375	88,663	16,33	5,2
		45-50	211	2,245	0,867	5,114	28,933	0,07	1,522	1,944	0,221	0,0266	1,8359	0,00576	0,01861	3,52391	96,476	15,36	5,3
	Profile 11	0-5	212	2,275	0,861	4,512	25,034	0,067	1,393	1,744	0,225	0,0303	1,7684	0,00535	0,01797	13,0164	86,984	16,91	5,5
		7-13	213	2,437	0,548	4,895	29,108	0,081	1,704	1,766	0,15	0,016	1,0818	0,00603	0,02425	4,93952	95,06	12,12	5,2
		15-20	214	2,528	0,618	5,055	28,627	0,096	1,696	1,851	0,186	0,0193	1,3347	0,00677	0,02189	4,79829	95,202	12,54	5,2
	Profile 12	0-5	215	2,069	1,653	4,959	26,705	0,11	1,42	1,968	0,373	0,0514	2,5967	0,00542	0,0191	5,36798	94,632	15,6	5,3
		38-43	216	2,066	1,177	5,096	25,731	0,138	1,392	1,972	0,308	0,0433	2,3314	0,00557	0,02062	5,57428	94,426	14,8	5,1

Appendix I 52: *Geochemistry, Site Charlie.*

		Depth [cm]	XRF-LOI [%]	Na	Mg	Al	Si	P	K	Ca	Ti	Mn	Fe	Rb	Zr	LOI Average [%]	Anorganic [%]	C/N	pH
Delta	Profile 3	0	26	2,647	0,941	5,881	32,012	0,036	1,6949	1,77	0,1546	0,0319	1,5816	0,00526	0,011371	2,31312	97,6869	17,444	5,2
		2,5	27	2,78	0,931	6,013	32,34	0,023	1,726	1,737	0,1636	0,0275	1,4607	0,00525	0,010622	1,37128	98,6287	14,241	5,25
		6	28	2,716	0,869	5,877	32,385	0,034	1,6769	1,766	0,1515	0,0265	1,4117	0,00519	0,012806	1,41535	98,5846	13,984	5,1
		8,5	29	2,795	0,881	5,91	32,451	0,023	1,6991	1,754	0,168	0,0303	1,5875	0,00523	0,01236	1,27436	98,7256	16,47	5,15
		11	30	2,777	0,914	6,037	32,891	0,022	1,6643	1,75	0,1613	0,0289	1,5133	0,00522	0,011727	1,28812	98,7119	16,558	4,9
		14	31	2,857	0,981	5,993	31,452	0,032	1,6659	1,792	0,1654	0,027	1,5039	0,00527	0,010366	1,83527	98,1647	15,991	4,75
		17	32	2,632	0,787	5,443	28,931	0,037	1,5146	1,776	0,1531	0,0252	1,5373	0,00516	0,011752	5,45277	94,5472	17,13	4,6
		20	33	2,343	0,694	4,604	23,908	0,055	1,3259	1,696	0,1286	0,016	1,2541	0,00490	0,012103	12,4257	87,5743	18,45	4,45
		22,5	34	2,366	0,693	4,767	26,672	0,053	1,4711	1,76	0,1494	0,017	1,2935	0,00504	0,014702	8,90767	91,0923	17,325	4,45
		25	35	2,388	0,624	4,771	26,593	0,083	1,5881	1,767	0,1594	0,0165	1,2414	0,00514	0,022349	8,51999	91,48	16,268	4,5
		28	36	2,28	0,649	4,94	26,906	0,055	1,6388	1,709	0,162	0,0258	1,3147	0,00545	0,020515	8,7	91,3	17,959	4,5
	Profile 3*	0-5	227	2,552	0,914	5,847	31,037	0,053	1,6023	1,749	0,1565	0,0271	1,5823	0,00542	0,013319	4,79512	95,2049	15,369	4,9
		46-51	228	3,338	0,824	7,249	31,92	0,012	1,9321	1,91	0,153	0,0273	1,53	0,00637	0,009263	0,71534	99,2847	11,205	5
	Profile 13	0	217	2,791	0,802	5,767	30,91	0,029	1,6163	1,791	0,1574	0,0286	1,5868	0,00531	0,011444	1,68567	98,3143	13,803	5,3
		5	218	2,86	0,782	5,817	31,388	0,029	1,6941	1,774	0,1382	0,0253	1,5476	0,00531	0,010707	1,04582	98,9542	15,884	5,2
		10	219	2,859	0,842	5,924	31,368	0,036	1,6307	1,831	0,1689	0,0285	1,7592	0,00538	0,010087	1,11106	98,8889	14,233	5,3
		15	220	2,715	0,731	5,678	31,155	0,046	1,655	1,808	0,1681	0,0258	1,5961	0,00551	0,013032	1,7202	98,2798	11,67	4,7
		20-25	221	2,651	0,637	5,552	31,531	0,058	1,7584	1,767	0,1687	0,0204	1,4221	0,00581	0,01906	2,25872	97,7413	12,312	4,5
	Profile 14	0-5	222	2,481	0,769	5,176	28,565	0,08	1,5469	1,787	0,1501	0,0416	1,4646	0,00530	0,015258	4,33601	95,664	13,102	5,15
		5-10	223	2,483	0,783	5,51	29,826	0,073	1,5454	1,775	0,1627	0,0538	1,612	0,00547	0,015762	3,47523	96,5248	11,792	4,35
		10-15	224	2,365	0,648	5,635	30,091	0,133	1,7767	1,759	0,1922	0,0502	1,5031	0,00610	0,022866	4,68599	95,314	13,371	4,25
	Profile 15	0-5	225	2,057	0,435	4,283	25,227	0,127	1,463	1,521	0,133	0,0163	1,1459	0,00520	0,02159	10,1925	89,8075	16,65	3,9
		15-20	226	3,995	1,335	8,856	37,07	0,037	1,8919	1,98	0,22	0,0308	1,9505	0,00797	0,016318	4,0127	95,9873	16,32	4,1

Appendix I 55: *Geochemistry, Site Delta.*

Appendix II: XRF graphs

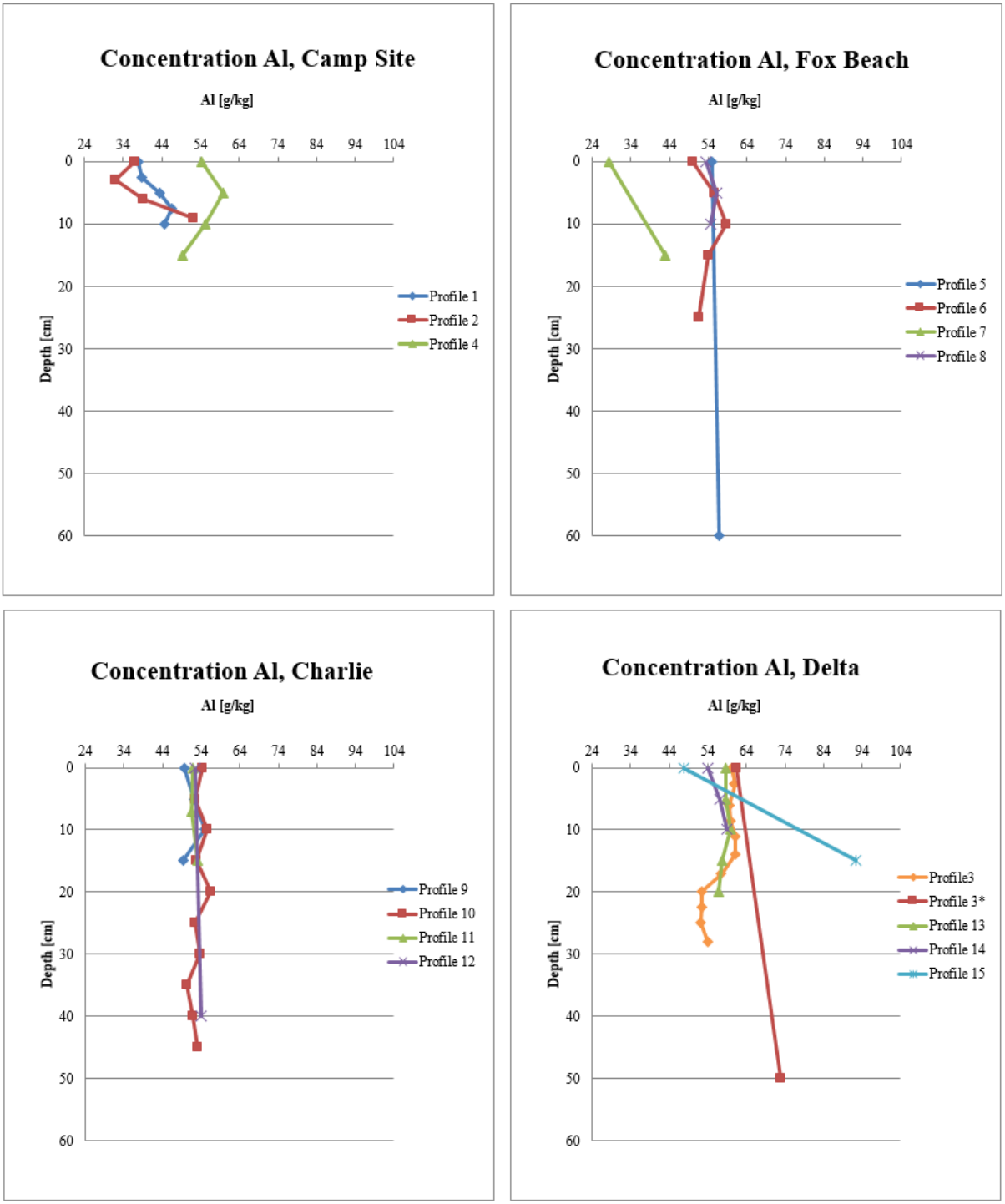

Appendix II 1: *Al-concentration at Camp Site, Fox Beach, Charlie and Delta. Profile 2, 8, 9, 3, 3* in the dead zone; Profile 7, 10, 13 in the affected zone; Profile 1, 6, 11, 14 in the transition zone; Profile 4, 5, 12, 15 in the reference zone.*

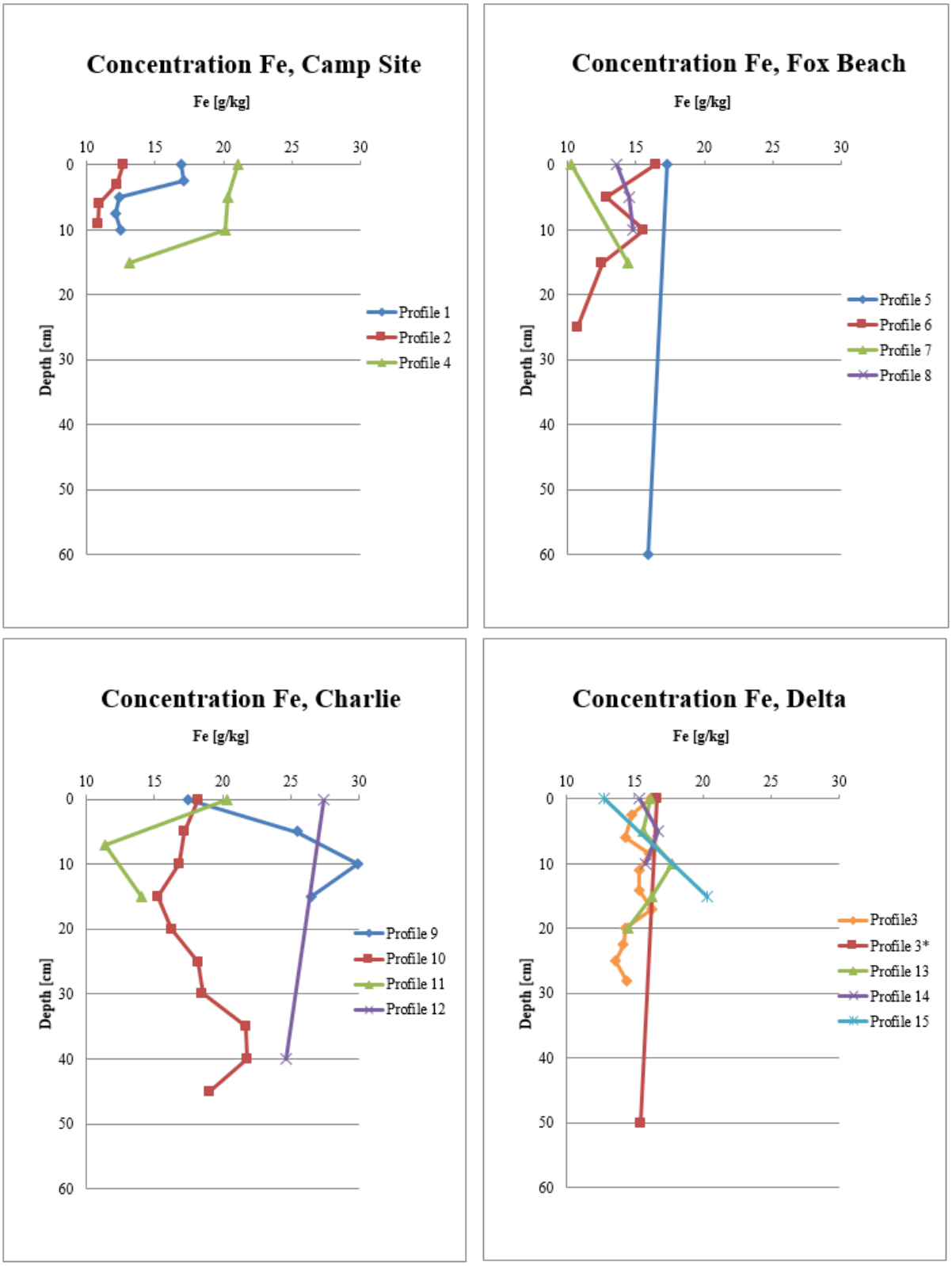

Appendix II 2: *Fe-concentration at Camp Site, Fox Beach, Charlie and Delta. Profile 2, 8, 9, 3, 3* in the dead zone; Profile 7, 10, 13 in the affected zone; Profile 1, 6, 11, 14 in the transition zone; Profile 4, 5, 12, 15 in the reference zone.*

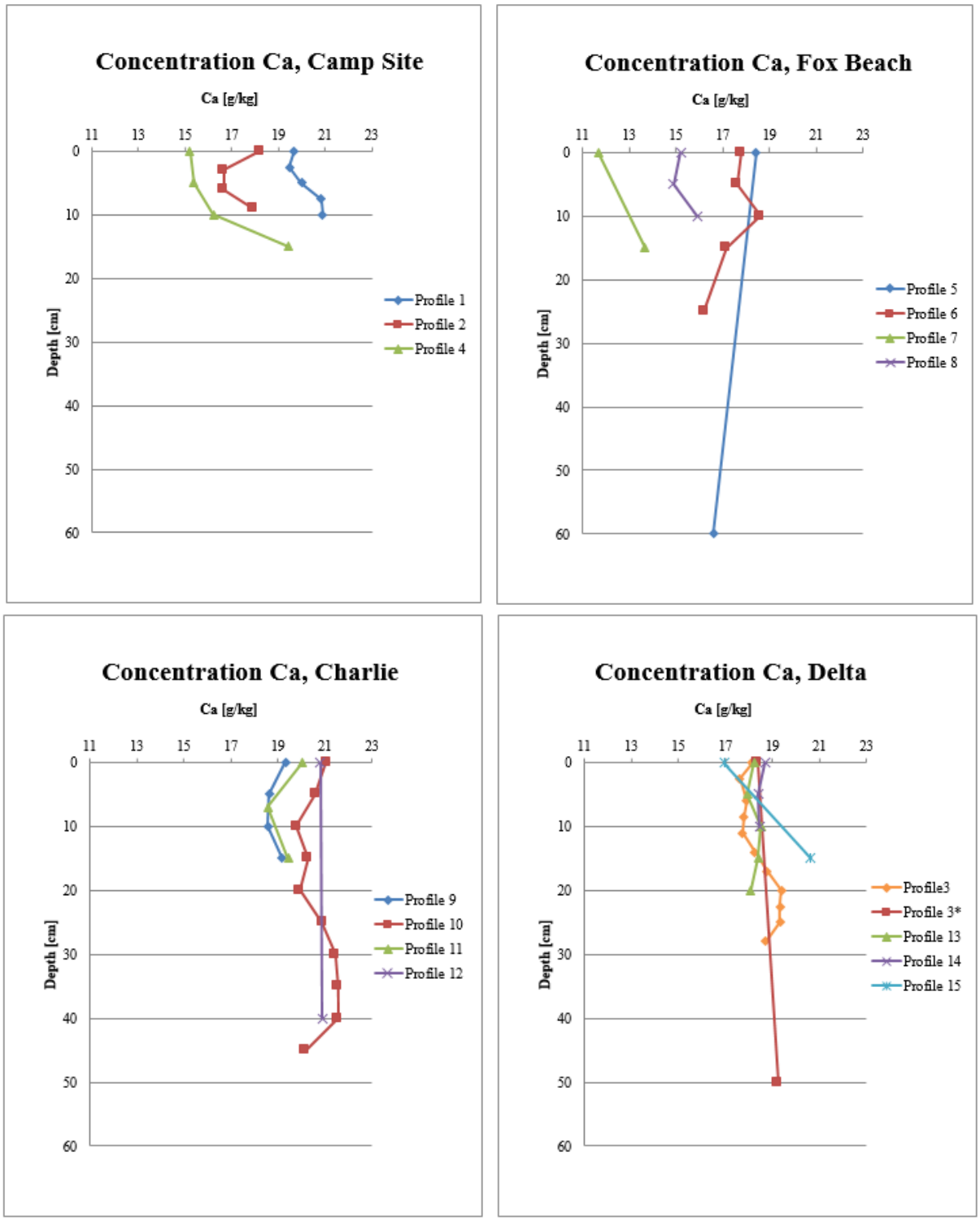

***Appendix II 3**: Ca-concentration at Camp Site, Fox Beach, Charlie and Delta. Profile 2, 8, 9, 3, 3* in the dead zone; Profile 7, 10, 13 in the affected zone; Profile 1, 6, 11, 14 in the transition zone; Profile 4, 5, 12, 15 in the reference zone.*

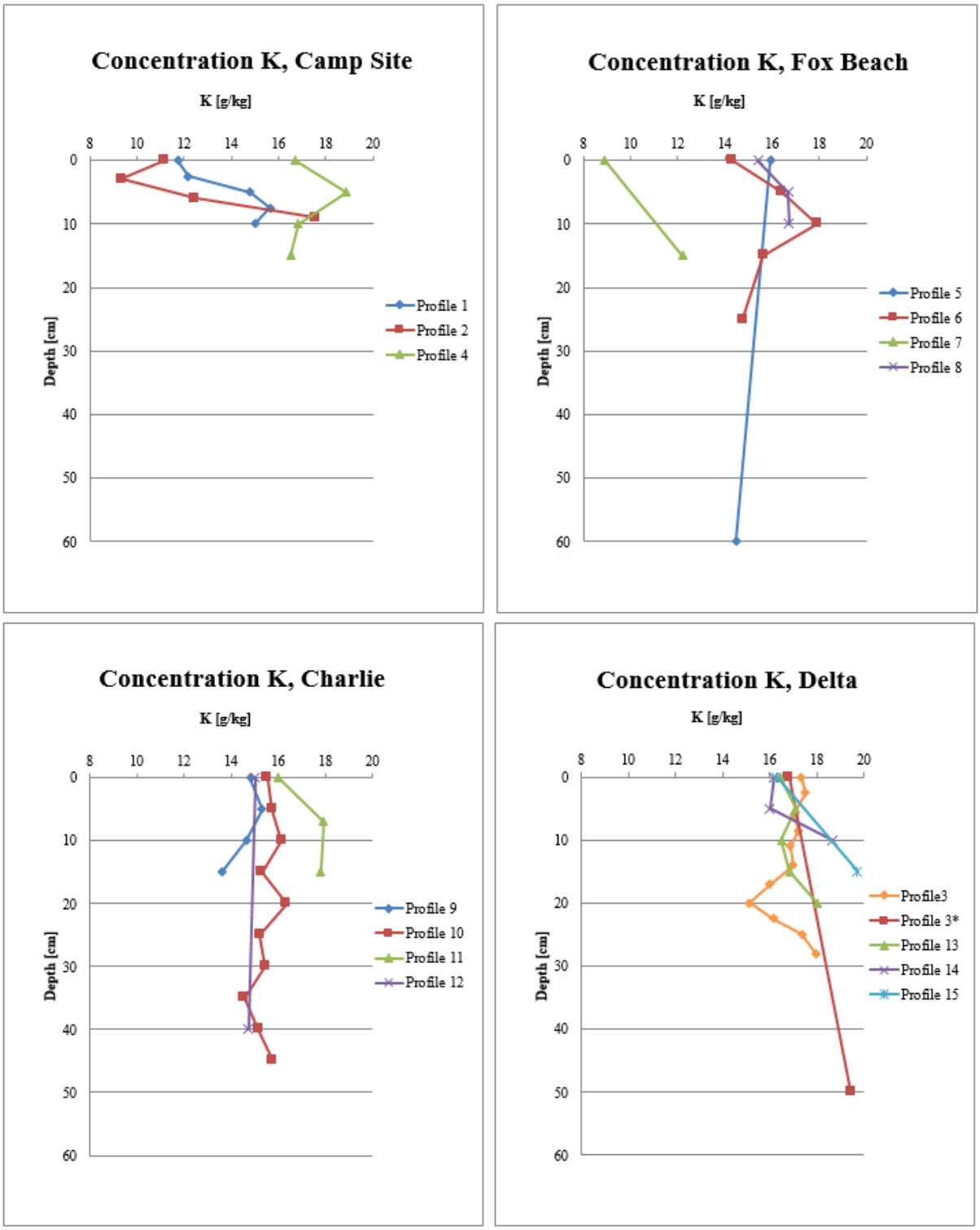

***Appendix II 4**: K-concentration at Camp Site, Fox Beach, Charlie and Delta. Profile 2, 8, 9, 3, 3* in the dead zone; Profile 7, 10, 13 in the affected zone; Profile 1, 6, 11, 14 in the transition zone; Profile 4, 5, 12, 15 in the reference zone.*

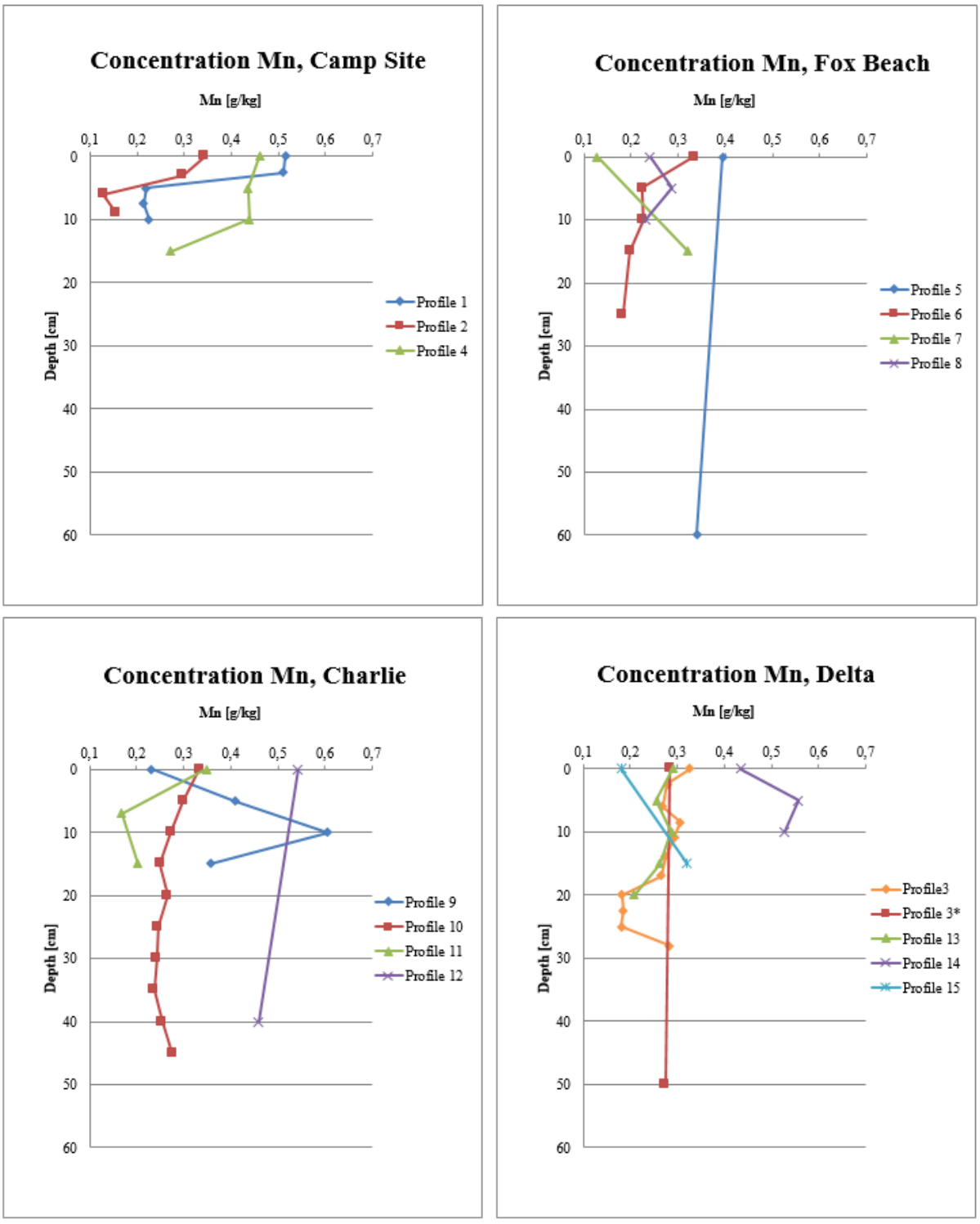

Appendix II 5: *Mn-concentration at Camp Site, Fox Beach, Charlie and Delta. Profile 2, 8, 9, 3, 3* in the dead zone; Profile 7, 10, 13 in the affected zone; Profile 1, 6, 11, 14 in the transition zone; Profile 4, 5, 12, 15 in the reference zone.*

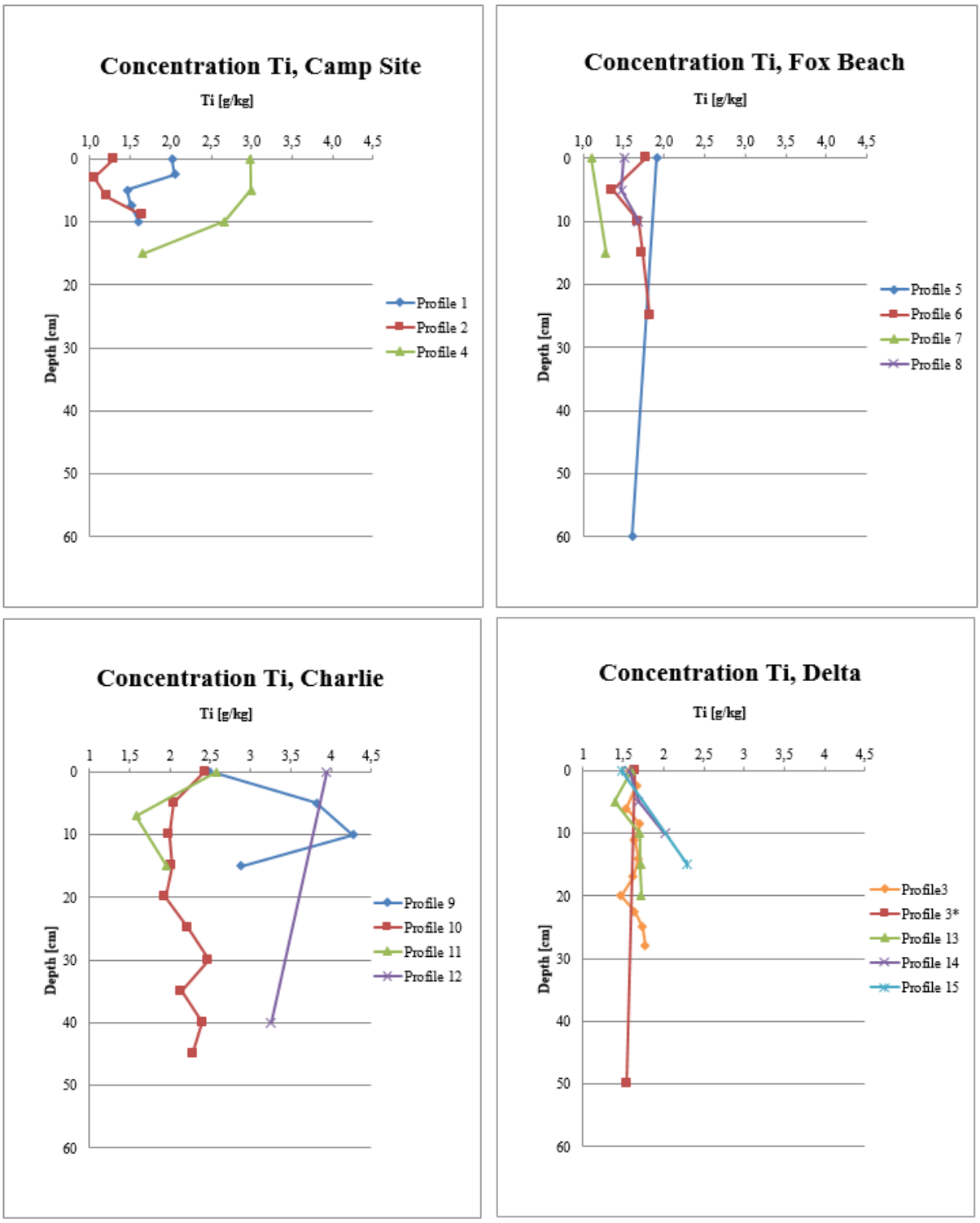

***Appendix II 6**: Ti-concentration at Camp Site, Fox Beach, Charlie and Delta. Profile 2, 8, 9, 3, 3* in the dead zone; Profile 7, 10, 13 in the affected zone; Profile 1, 6, 11, 14 in the transition zone; Profile 4, 5, 12, 15 in the reference zone.*

Appendix III: ^{14}C Oxcal Calibrations

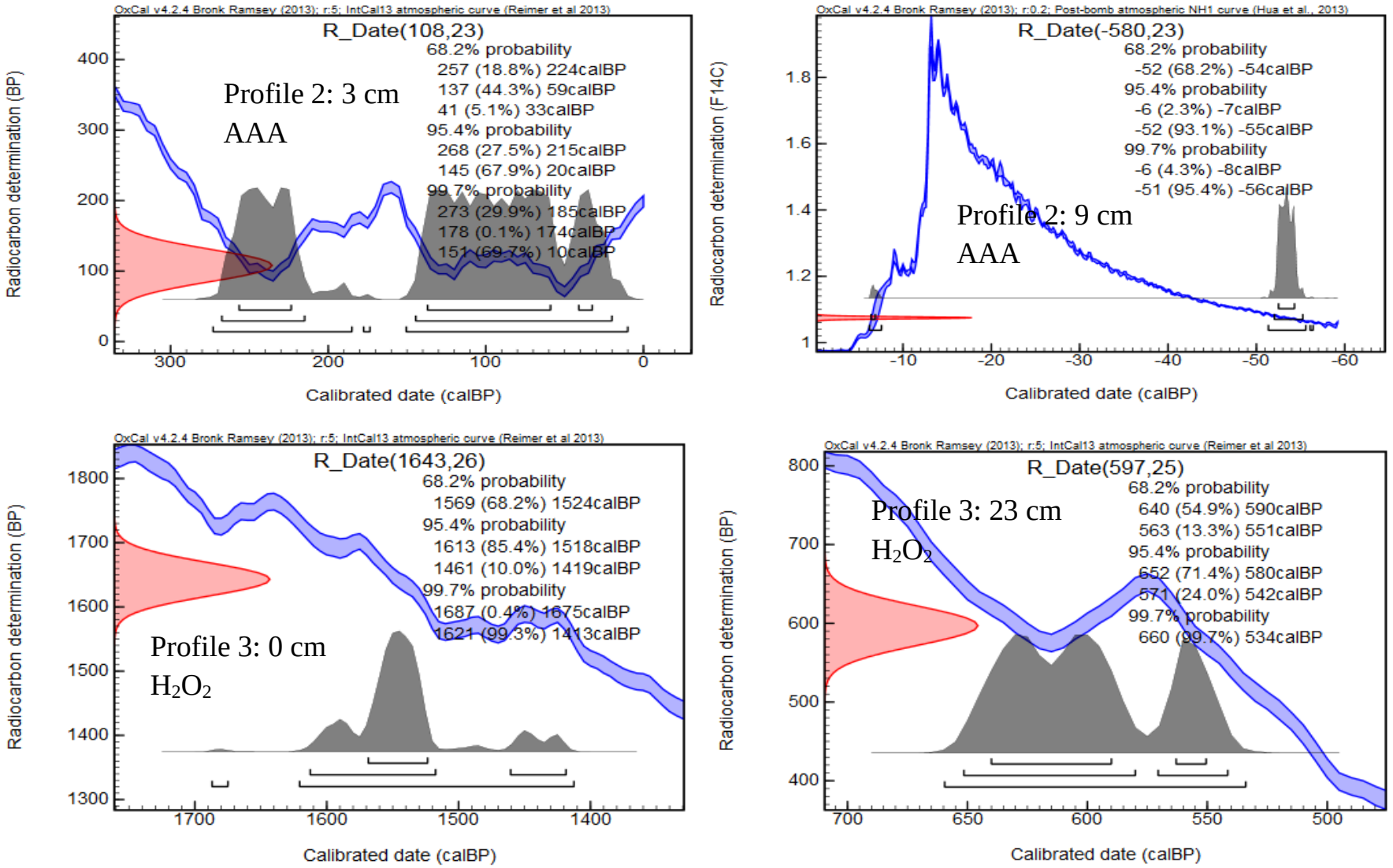

Appendix III 1: *^{14}C Oxcal Calibrations. Profile 2 and 3.*

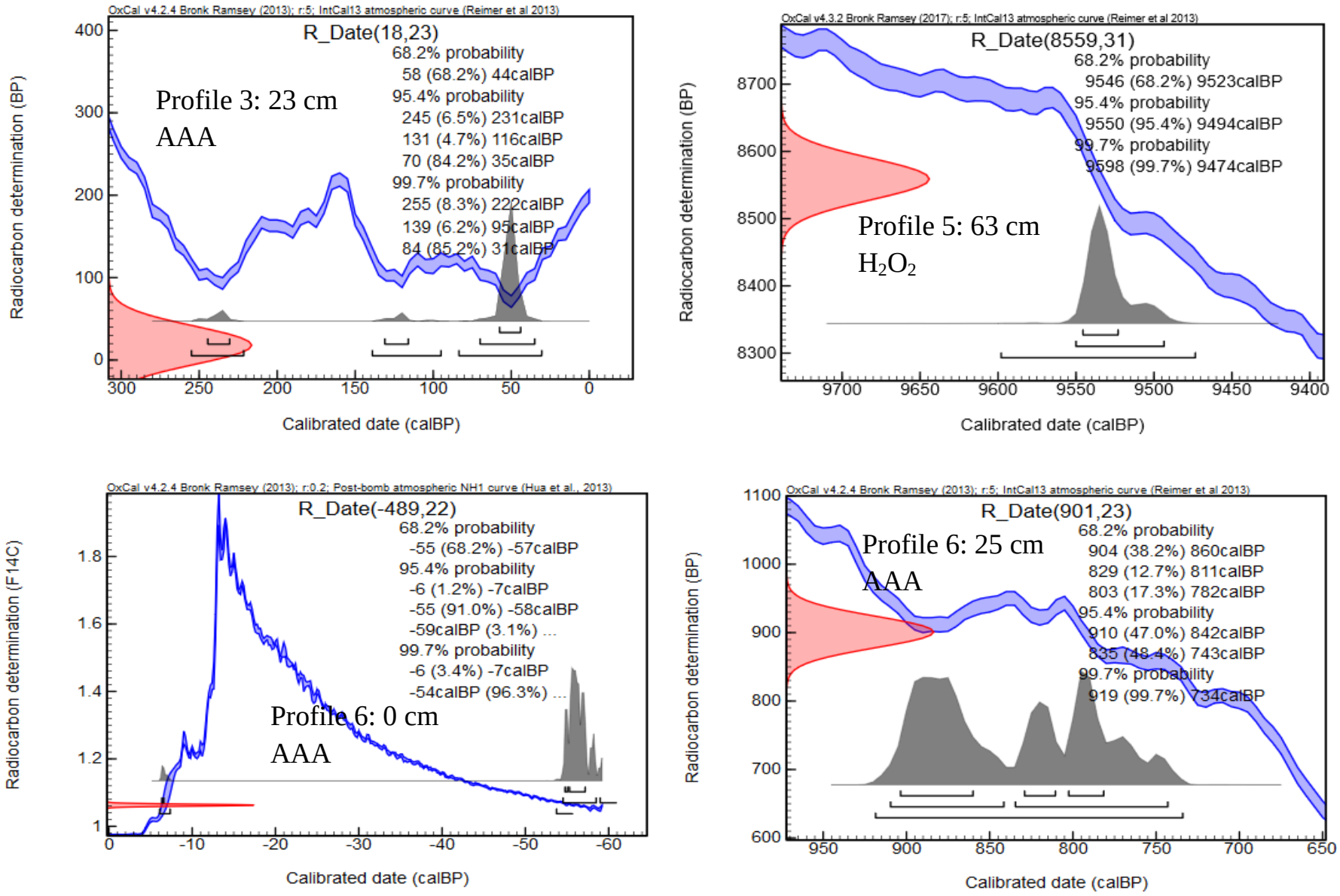

Appendix III 2: *^{14}C Oxcal Calibrations. Profile 3, 5 and 6.*

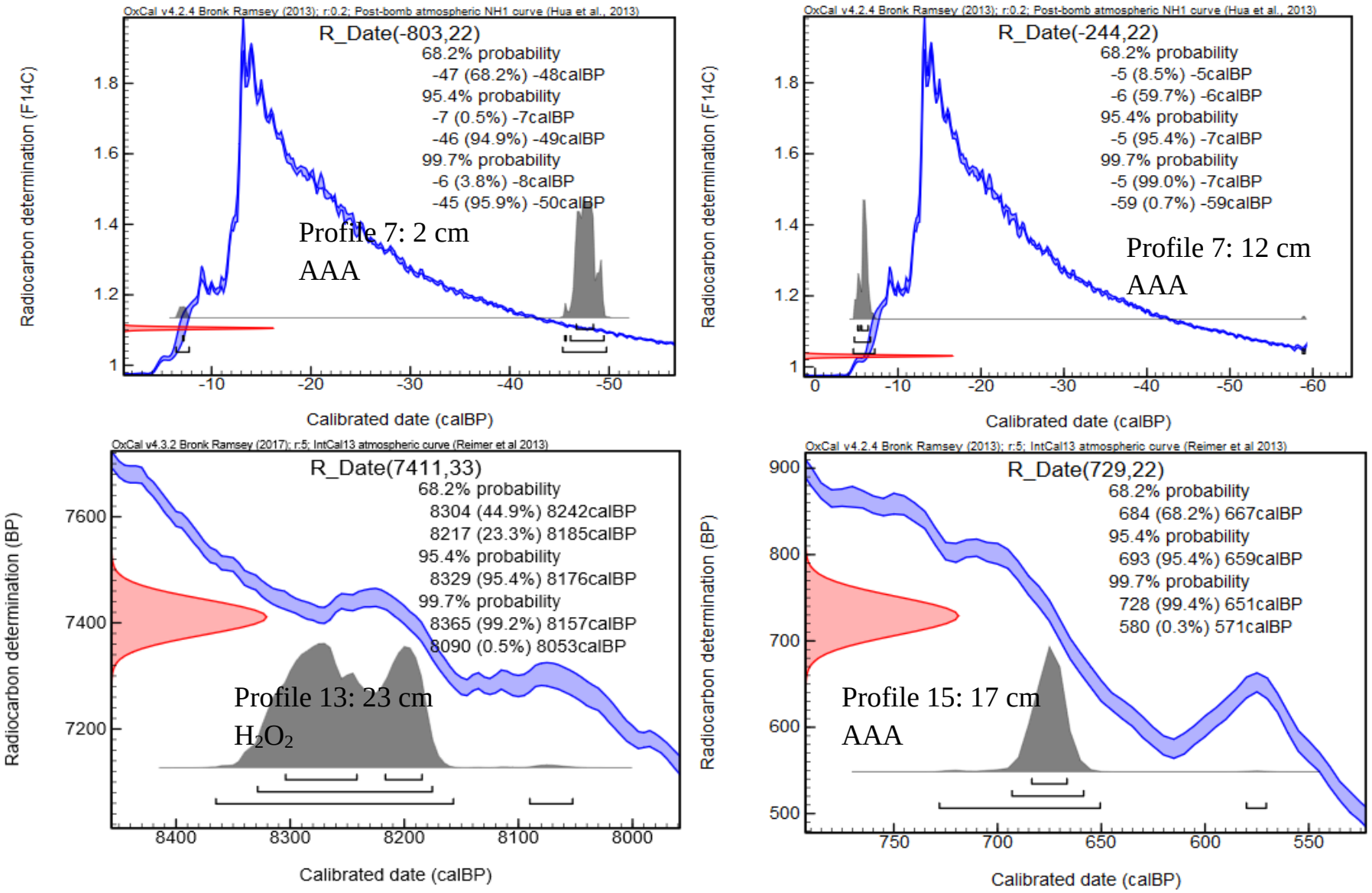

Appendix III 5: *^{14}C Oxcal Calibrations. Profile 7, 13 and 15.*

10. Personal declaration

I hereby declare that the submitted thesis is the result of my own, independent work. All external sources are explicitly acknowledged in the thesis.

Zürich, September 2017

Larissa Lucille Sutter

11. Acknowledgements

First, I would like to thank Prof. Dr. Markus Egli for his big support and help at any time in the laboratory or during meetings. His reliable and patient way makes him to an outstanding supervisor. Second, I thank Prof. Dr. Andreas Vieli for supporting me during my thesis and helping me digging holes and collecting dwarf shrubs in Greenland. Of course, also a special thank goes to Dr. Holger Gärtner. He was there for me when I had any questions about my dwarf shrubs or dendrochronological issues. Also, I would like to say thank you to Dr. Martin Lüthi for organizing the whole excursion to Greenland.

Further, I would like to say thank you to Sandra Röhtlisberger, Ivan Woodhatch and Thomas Keller, who enabled my analysis in the laboratory at the University of Zürich. Some thanks, also to Anne Verstege, Daniel Nievergelt, who were supportive during my work at the WSL in Birmensdorf. An appreciative thank is written to Loïc Schneider for his technical assistance at the WSL.

A very special thank is addressed to SEP (the swiss organization of snow, ice and permafrost) for their generous grants, which made the excursion to Greenland possible.

Last but not least, I owe my success of this master's thesis and my study to my loving family, Reto, Denys and Leah Sutter, who encouraged and supported me at all time.